reactions

MDPI

Review

Smart Designs of Anti-Coking and Anti-Sintering Ni-Based Catalysts for Dry Reforming of Methane: A Recent Review

Xingyuan Gao [1,2,3], Jangam Ashok [3] and Sibudjing Kawi [3,*]

[1] Department of Chemistry, Guangdong University of Education, Guangzhou 510303, China; gaoxingyuan@gdei.edu.cn
[2] Engineering Technology Development Center of Advanced Materials & Energy Saving and Emission Reduction in Guangdong Colleges and Universities, Guangzhou 510303, China
[3] Department of Chemical and Biomolecular Engineering, National University of Singapore, Singapore 117585, Singapore; chejang@nus.edu.sg
* Correspondence: chekawis@nus.edu.sg

Received: 3 November 2020; Accepted: 9 December 2020; Published: 14 December 2020

Abstract: Dry reforming of methane (DRM) reaction has drawn much interest due to the reduction of greenhouse gases and production of syngas. Coking and sintering have hindered the large-scale operations of Ni-based catalysts in DRM reactions at high temperatures. Smart designs of Ni-based catalysts are comprehensively summarized in fourth aspects: surface regulation, oxygen defects, interfacial engineering, and structural optimization. In each part, details of the designs and anti-deactivation mechanisms are elucidated, followed by a summary of the main points and the recommended strategies to improve the catalytic performance, energy efficiency, and utilization rate.

Keywords: Ni-based catalysts; dry reforming of methane; anti-coking; anti-sintering

1. Introduction

Many studies have been focused on the conversion of CO_2 and CH_4 (two greenhouse gases) to value-added chemicals or petrochemicals in various processes, such as reforming of methane [1–8], CO_2 methanation [9–16], membrane-assisted reaction [17–21], chemical looping [22], reversed water-gas-shift [23,24], and catalytic decomposition [25]. Therein, dry reforming of methane (DRM) reaction draws much interest because it contributes to the reduction of greenhouse gases (CO_2 and CH_4) and generates a mixture of CO and H_2 (syngas), which can be used as fuels and further converted to high value-added petrochemicals [26–31]. The reaction equation is shown as below:

$$CH_4 + CO_2 \leftrightarrow 2CO + 2H_2 \qquad \Delta H_{298K} = 261\ kJmol^{-1} \tag{1}$$

The low H_2:CO ratio is favorable to Fischer–Tropsch reaction due to the promotion of chain growth and suppression of methanation. Also, the endothermic forward reaction benefits the Solchem process by converting solar energy to chemical energy. Moreover, DRM reaction is applicable for the storage of seasonal energy in the form of CO and H_2 [32–35].

In order to activate the reactants, noble metal catalysts are applied and proved to be highly reactive. However, the high cost, low abundance, and metal sintering hinder their large-scale applications in industry [30]. Ni-based catalysts have been widely studied due to their low cost and good activities, but carbon deposition, metal sintering, and surface oxidation lead to the deactivation of catalysts and impede their further applications [30]. For example, the in situ XPS technique was applied to monitor the evolution of Ni surface during the reaction. Results showed that during the inactive period, 3 nm

layer of NiO covered the metallic Ni surface, leading to the decrease of reactivity [36]. Solutions have been provided to address this issue, including the size control of active metals, doping second transition element, adding alkali earth or rare earth promoters to the support, tuning metal-support interaction (MSI), structure designs and optimization of reaction parameters [26–31]. Researchers have reviewed the progress of Ni-based catalysts for DRM reaction in terms of the metal doping, porous supports, and kinetics/mechanisms, which shows the high importance of and widespread attention paid towards the DRM reaction [26–31]. However, it is rare to see a summary of the structure designs of supports, architectures of the catalysts, surface species control and interfacial strength adjustment in recent years, which greatly affects the active surface area, activities, and anti-deactivation capabilities. In this review, we summarize the recent advances of Ni-based catalysts' modifications and corresponding catalytic performances for DRM reaction. The following parts consist of surface regulation, oxygen defects, interfacial engineering, and structural optimization, followed by concluding remarks and prospects.

2. Surface Regulation

For most heterogeneous reactions, reactants are adsorbed and activated on the surface active sites to produce the intermediates and final products. Modifying the surface properties has significant effects on the catalytic process and performances. In DRM reaction, CO_2 and CH_4 are converted to CO and H_2 through adsorption, dissociation, and recombination on the surface of Ni-based catalysts. Surface basicity exerts a great influence on the catalytic conversions and coke resistance [30].

Surface acidity and basicity affect the electron environment of metal active sites and the adsorption of reactants, thus determining the catalytic performances. For example, Lewis acid sites reduce electron density of Ni species and balance the activation of CH_4 and removal of carbon deposits, leading to a high stability in DRM reaction [37]. Also, enhanced basicity of the supports improves the adsorption of CO_2, which subsequently dissociates into CO and oxygen atoms, reacting with the decomposition intermediate CH_x to produce CO and inhibit carbon formation [30]. To enhance the surface basicity, various compounds have been utilized, including alkali and alkali earth metal oxides and rare earth metal oxides [30,38–41].

La_2O_3 as a rare earth metal oxide, acts as the support to promote the adsorption of CO_2 by reacting with CO_2 to form La oxycarbonate ($La_2O_2CO_3$) [42]. According to in-situ DRIFT study, carbon species from the activation of methane reacted with the La oxycarbonate to form CO, removing the surface coke and maintaining the active sites [43]. The reaction mechanism was shown as below [43]:

$$CH_4 + * \leftrightarrow * - CH_4$$

$$CO_2 + La_2O_3 \leftrightarrow La_2O_2CO_3 \text{ (RDS)}$$

$$* - CH_4 \rightarrow * - C + 2H_2$$

$$La_2O_2CO_3 + C - * \rightarrow La_2O_3 + 2CO + * \text{ (RDS)}$$

To further enhance the CO_2 adsorption, MgO as a basic oxide is promising due to its successful applications [44–47]. When MgO was added into the Ni/La_2O_3, due to its strong basicity, more CO_2 adsorbed on the surface to react with La_2O_3 to form monoclinic $La_2O_3CO_3$. Interestingly, at a low Mg:La ratio, only hexagonal La_2O_3 and $La_2O_2CO_3$ mixtures were formed, which was not effective as monoclinic phase in reacting with carbon species, thus deactivating the catalysts much faster (seen in Table 1) [48]. To further elucidate the mechanism of removing the carbon deposits by La_2O_3, a theoretical study was conducted to compare the different catalytic pathways of La_2O_3 and La metal. La_2O_3-Ni followed the reaction pathway below: $CH_4 + CO_2 + La_2O_3 \rightarrow CH + CO_2(La_2O_2\text{-}O) + 3H \rightarrow CHO + CO_2(La_2O_2) + 3H \rightarrow 2CO + 2H_2 + La_2O_3$. It showed that the oxygen atom dissociated from La oxycarbonate reacted with CH or C species to form CO. On the other hand, La metal dopant was not effective as the oxide since the faster rate of $CH \rightarrow C + H$ for La-Ni accelerated the coke formation than La_2O_3-Ni catalysts [49]. As another rare earth metal oxide, CeO_2 may decrease the

total basicity. However, the intermediate and strong basic sites could be enhanced, thus promoting the CO_2 adsorption and modifying the activity (shown in Table 1) [50].

Besides La_2O_3, CeO_2 and MgO, other group metal oxides can also enhance the surface basicity. Considering the acidity of SiO_2 support, Ga_2O_3 (Table 1) was added as a promoter to enhance the basicity and facilitate the adsorption of CO_2 to form carbonate or bicarbonate species (Figure 1), which reacted with carbon deposits more easily than the physically or linearly adsorbed CO_2 on the pristine SiO_2 surface [51].

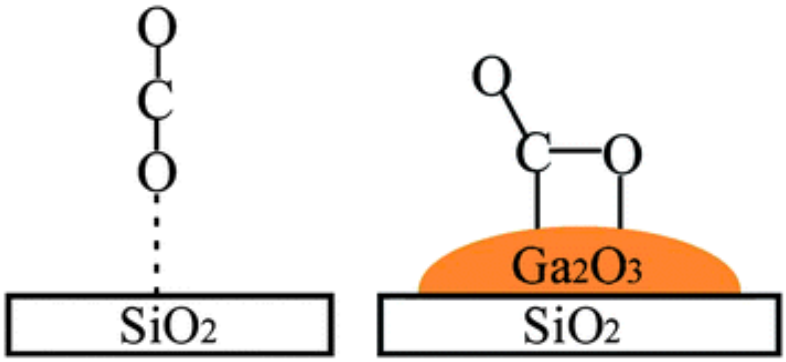

Figure 1. Activation of CO_2 on Ga_2O_3-promoted SiO_2 support. Reproduced with permission from reference [51].

B_2O_3 as a non-metal oxide has been successfully doped into Ni/Al_2O_3 to enhance the surface hydroxyl group concentrations. The borated surface was rich in OH group which promoted the oxidation of carbon deposits from CH_4 decomposition [52].

In certain situation, if the basicity of the support is too strong, the CO_2 adsorption may not inhibit but lead to carbon deposition [53]. As shown in Table 1, to alleviate the basicity of Ni supported on MgO/Al_2O_3, Y_2O_3 was added to introduce more weak and medium basic sites on the surface [54,55]. By using 1.5 wt% of Y_2O_3, the highest conversion of CH_4 and CO_2 was achieved with the best stability [54]. In addition, La-promoted Ni–Mg–Al hydrotalcite was reported to be anti-coking due to the gasification of carbon deposits where weak and medium basic sites were increased [56].

In a word, adding promoters like MgO, La_2O_3 and Ga_2O_3 could enhance the surface basicity, thus facilitating the adsorption of CO_2 which dissociated into CO and O and removed carbon deposits. Besides the surface basicity adjustment, surface hydroxyl group concentrations could be increased by adding B_2O_3 as a promoter, which promoted the carbon oxidation and maintained the stability. But a careful control of the surface basicity may be necessary since a too strong basicity could not inhibit the coke formation.

Table 1. A summary of surface regulation effects on the catalytic performances of Ni-based catalysts for DRM reaction.

Catalyst [a)]	Preparation Method	Reaction Condition	Methane Conversion	CO_2 Conversion	Carbon Formation	Comments	Ref.
Ni/La_2O_3	Wet impregnation method	700 °C; $CH_4/CO_2 = 1$	70% for CH_4 after 50 h	75% for CO_2 after 50 h	10.3%	Carbon species reacted with the La oxycarbonate to form CO.	[42]
$Ni/MgO\text{-}La_2O_3$	Co-precipitation and impregnation method	700 °C; $CH_4/CO_2 = 1$	63% for CH_4 after 200 h	65% for CO_2 after 200 h	0.031 mol_C/mol_{CH4}	When MgO was added into the Ni/La_2O_3, more CO_2 adsorbed on the surface to react with La_2O_3 to form monoclinic $La_2O_3CO_3$.	[48]
Ce-NiMgAl	Co-precipitation method	550 °C; $CH_4/CO_2 = 1$	54.8% for CH_4 after 5 h	37.4% for CO_2 after 5 h	Around 90%	CeO_2 enhanced the amount of medium and strong basic sites.	[50]
$Ni/SiO_2–Ga_2O_3$	Incipient wetness impregnation method	700 °C; $CH_4/CO_2 = 1$	70% for CH_4 after 10 h	79% for CO_2 after 10 h	16.8 mg/g_{cat}	Ga_2O_3 was added as a promoter to enhance the basicity to facilitate the adsorption of CO_2 to form carbonate or bicarbonate.	[51]
$5\%Ni/B_2O_3–Al_2O_3$	Impregnation method	700 °C; $CH_4/CO_2 = 1$	75% for CH_4 after 65 h	67% for CO_2 after 65 h	13%	The borated surface was rich in OH group which promoted the oxidation of carbon deposits.	[52]
HTNi-Y	Co-precipitation method	700 °C; $CH_4/CO_2 = 1$	74% for CH_4 after 10 h	78% for CO_2 after 10 h	75.8%	Y_2O_3 was added to introduce more weak and medium basic sites on the surface.	[54]
Y-NiMgAl	Co-precipitation method	700 °C; $CH_4/CO_2 = 1$	85% for CH_4 after 5 h	90% for CO_2 after 5 h	35.1%	Basicity increased with the increase loading of Y.	[55]
La-NiMgAl	Co-precipitation method	550 °C; $CH_4/CO_2 = 1$	45% for CH_4 after 8 h	37% for CO_2 after 8 h	87.5%	La dopant enhanced the content of medium and weak basic sites.	[56]

[a)] HT: hydrotalcite.

3. Oxygen Defects

In addition to the surface basicity and acidity regulation, oxygen defects including lattice and surface oxygen and oxygen vacancies enhance the oxygen mobility and adsorption, which effectively removes the carbon deposits during DRM reaction [30]. Rare earth metal oxides, transition metal oxides, mixed oxides, and perovskites will be discussed as below based on the origin of oxygen defects and corresponding effects on the carbon removal.

3.1. Rare-Earth Metal Oxides

Studies have shown that rare earth metal oxides can generate oxygen defects, promote oxygen mobility, and scavenge carbon species [57–77]. As the representative, CeO_2 with a good redox property can release lattice oxygen to generate oxygen vacancies, thus accelerating the oxygen mobility. When CeO_2 was used as the support for Ni metals, the catalytic performance benefited from the lattice oxygen defects of CeO_2 and the reversible conversion between Ce^{3+} and Ce^{4+}. When Ce^{4+} was reduced to Ce^{3+}, lattice oxygen was released and oxygen vacancies were formed, which improved the adsorption of oxygen species like O_2 or CO_2 to generate oxygen radicals, thus reducing the carbon deposition on the surface. However, an excessive amount of CeO_2 may cover the Ni active sites and lower the accessibility of reactants to the Ni metal surface, causing a low conversion of CH_4 and CO_2 [30,65,78,79].

Theoretical study was applied to explore and elucidate the role of CeO_2 in Ni catalysts for DRM reaction. Results showed that the activation sites for CH_4 and CO_2 were different. For CH_4 activation, the preferred sites included metal-support interface, oxygen vacancies at the metal-support interface and the metal vacancies. But for CO_2, the reactant molecule was mostly adsorbed and dissociated at oxygen vacancies at either the support or the metal-support interface. Moreover, the active sites could be regenerated by the interfacial oxygen of CeO_2, maintaining the stability of the catalyst [58]. The detailed mechanistic diagram is shown in Figure 2 below.

Another possible explanation of the catalytic effect of CeO_2 was presented as below:

$$CeO_2 + nCH_4 \rightarrow CeO_{2n} + nCO + 2nH_2 \quad (2)$$

$$CeO_{2-n} + nCO_2 \rightarrow CeO_2 + nCO \quad (3)$$

The lattice oxygen of CeO_2 reacted with CH_4 to produce CO and H_2, leaving a ceria with oxygen defects, which subsequently grabbed oxygen atoms from CO_2 to recover to CeO_2 and produce another molecule of CO. The initial high oxidation state of Ce ion is essential to the whole process. However, during the DRM reaction, the existence of hydrogen possibly reduced Ce^{4+} to Ce^{3+}, decreasing the conversion of CH_4 and CO_2. Therefore, the immediate removal of hydrogen product from the system determines the catalytic effect of CeO_2 [80].

To stabilize the CeO_2 in the Ni catalysts, ZrO_2 can be added to substitute the Ce in the lattice to form a cubic phase of $Ce_xZr_{1-x}O_2$. This structure contains more oxygen vacancies and higher oxygen storage capacities than tetragonal phase. Because of the enhanced oxygen release capability, carbon deposits around the oxides are easily oxidized to form CO [81]. Likewise, as seen in Table 2, in another catalyst of Ni supported on CeO_2-ZrO_2 mixed oxides, the bonding degree determined the amount of oxygen vacancies. Also, the different oxidation states of Ce and Zr produced more oxygen vacancies. With the increase of Ni concentration, oxygen vacancies increased accordingly. When Ni reached the optimal molar ratio (9.3 mol%), the highest conversion of CH_4 and CO_2 was achieved [82].

Besides CeO_2, Y_2O_3 is also proved to be effective in removing the carbon deposits due to its surface oxygen mobility. During the DRM reaction, the movement of surface oxygen was accelerated with the generation of interstitial oxygen ions when lattice defects were produced in Y_2O_3. Interestingly, Y_2O_3 with a smaller crystal size exhibited a higher surface oxygen mobility, thus decreasing the carbon formation rate [57]. In another study shown in Table 2, α-oxygen was found on the surface of

Y_2O_3 to activate CH_4 and remove the carbon. Considering the limited amount of α-oxygen, it was necessary to feed a small amount of oxygen to maintain the stability of the catalyst by regenerating the α-oxygen [83].

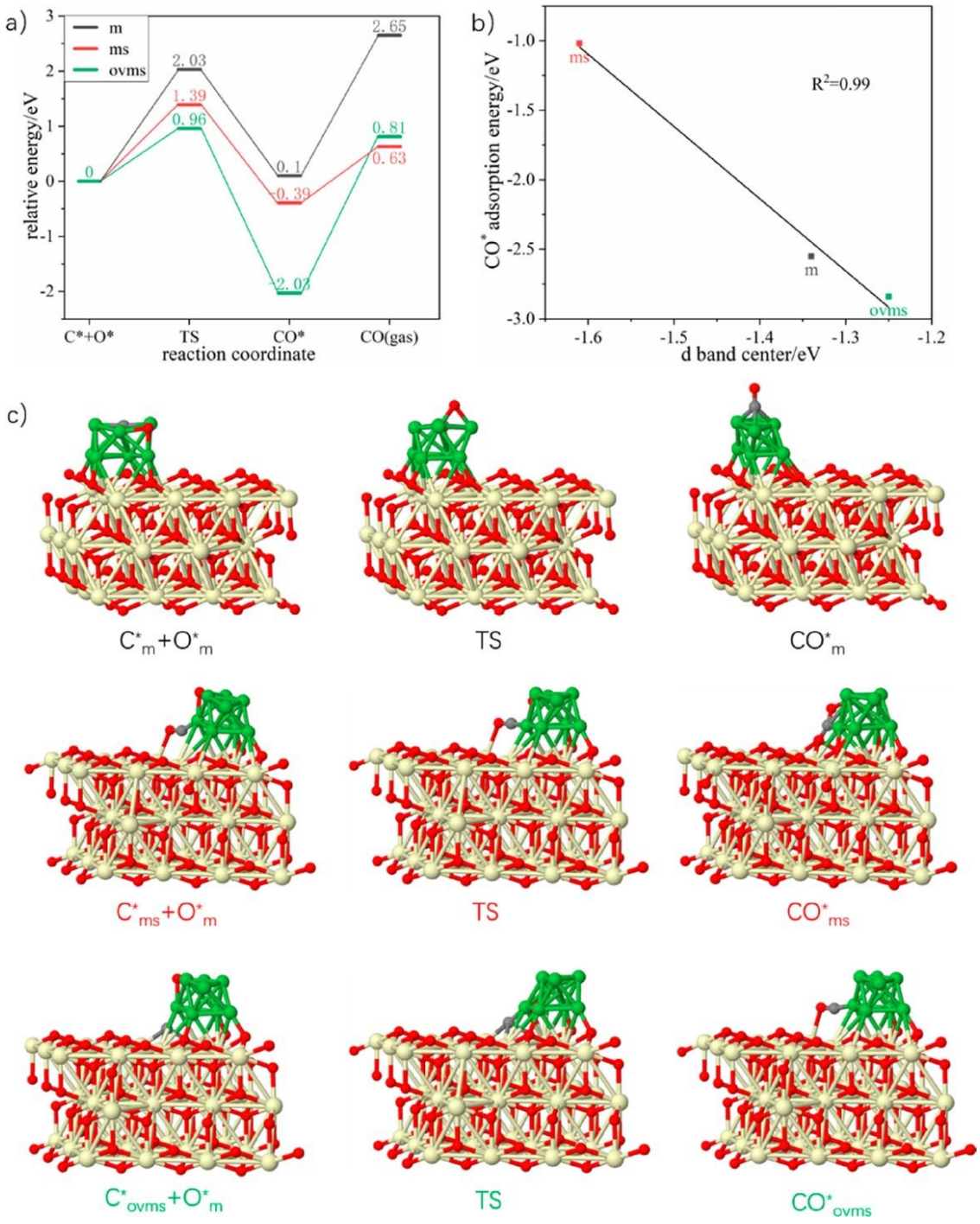

Figure 2. Three paths of C* elimination. (**a**) Relative energy of C* elimination at m, ms, and ovms sites. (**b**) Relation of d band center with CO* adsorption energy. (**c**) Corresponding configurations of part a. Gray spheres represent C, red spheres represent O, green spheres represent Ni and cream-colored spheres represent Ce. Reproduced with permission from reference [58].

Another rare earth metal oxide La_2O_3 also draws attention in recent years as a promoter for Ni catalysts to inhibit coke formation in DRM reaction. As presented in Table 2, besides the effect of

La oxycarbonate formed with adsorbed CO_2 mentioned previously, the addition of small amount of Sr could enhance the surface oxygen species mobility, which facilitated the C-H activation and coke removal, leading to a high CO_2 conversion and low carbon formation even at 600 °C reaction temperature [84].

In addition to the mixed oxides of CeO_2 and ZrO_2 above, two rare earth metal oxides can also be mixed to form a support for Ni catalyst, such as $Ce_{0.70}La_{0.20}Ni_{0.10}O_{2-\delta}$. During the reaction, the lattice of CeO_2 expanded due to the partial dissolution of La^{3+} into the lattice structure to generate oxygen vacancies. Moreover, with the increase of reduction temperature, the change of Ce oxidation state further increased the amount of oxygen vacancies. Under the condition of GHSV = 26,400 h^{-1}, no carbon deposition was found, demonstrating the excellent coke resistance (seen in Table 2) [85].

In a word, owing to the redox property and high oxygen storage capacity, rare earth metal oxides can produce oxygen defects (vacancies) with the change of oxidation state and release of oxygen atoms. With the addition of second metals, the synergetic effect may generate more oxygen defects so that the activation of CH_4 and CO_2 as well as the carbon removal can be enhanced simultaneously, leading to the high activity and stability of Ni catalysts for the DRM reaction.

3.2. Transition Metal Oxides

Due to the incompletely occupied d orbitals, transition metal oxides have been widely studied as a support to enhance the coke resistance by producing lattice oxygens to reduce the carbon depositions during DRM reaction. ZrO_2 and TiO_2 are two representatives which will be discussed in detail below [86–89]. As for Fe, considering its main existing form as a Ni-Fe alloy instead of metal oxides, the effect of Fe will be illustrated in the interfacial engineering part.

The lattice oxygen species of ZrO_2 plays a crucial role in the anti-coking property of Ni catalysts in DRM reaction. As seen in Table 2, the results of XRD and XPS showed that CH_4 decomposed into CH_x fragments and H atoms. The latter combined with each other to produce H_2; the former adsorbed on the Ni metal to form $NiCH_x$ species. Because of the intimate interaction between Ni and ZrO_2, the lattice oxygen of ZrO_2 reacted with CH_x to form CO and H_2 and regenerated the Ni active sites. In the meanwhile, the coke formation was inhibited due to the release of lattice oxygen of ZrO_2 and its affinity for the CO_2 adsorption [59].

To enhance the interaction between Ni and ZrO_2, a core-shell structure of Ni-ZrO_2@SiO_2 was prepared by hydrolysis of TEOS to form a mesoporous SiO_2 shell and thermal treatment of $NiZr(OH)_x$ to form a Ni-ZrO_2 core as shown in Figure 3. More active sites were formed at the interface and perimeter of Ni-ZrO_2 with the stabilization effect of ZrO_2 on Ni. As presented in Table 2, more abundant active oxygen provided by ZrO_2 easily accessed the carbon species at Ni active sites and oxidized the coke to form CO, maintaining the stability of the catalyst [89].

In order to elucidate the effect of different oxygen species in ZrO_2 on the carbon removal for Ni catalysts in DRM reaction, three types of calcination atmospheres were applied. Results showed that the optimal ratio of surface adsorbed oxygen to lattice oxygen was achieved under H_2 treatment, most favorable for CO_2 and CH_4 adsorption and activation, thus leading to the highest conversions and stability. Relative speaking, catalysts calcined under N_2 and oxidizing atmospheres presented a lower ratio of surface oxygen to lattice oxygen, suffering from the serious carbon formation shown in Table 2 [90].

Besides ZrO_2, another transition metal oxide TiO_2 is proved to be effective in removing the carbon due to the lattice oxygen. Two oxygen species were found in TiO_2, that is, oxygen ions inside TiO_2 and lattice oxygen at the interface. The later could react with the coke formed on the surface of Ni to produce CO, thus maintaining the active surface area for the reactants to continue dissociation. Moreover, water vapor provided by the humid environment showed a high affinity for the oxygen vacancies and dissociated on TiO_2 to reduce the carbon deposits [86].

Figure 3. Illustration of the fabrication method of the Ni-ZrO_2@SiO_2 catalyst with ultra-high coking and sintering resistance for the DRM reaction. Reproduced with permission from reference [89].

In a word, the lattice oxygen of ZrO_2 and TiO_2 can react with surface carbon species such as CH_x and carbon deposits to form CO. A careful control of the ratio between surface and lattice oxygen may affect the coke resistance. Further strengthening the MSI can lead to the intimate contact between abundant oxygen species and carbon residues, resulting in a high conversion and low carbon deposition.

3.3. Perovskites

Represented by the formula ABO_3, perovskite structures have been widely investigated in heterogeneous catalysis at high temperatures due to its good thermal stability [91–97]. By substitution of A-site ions, the dimension of unit cells changes, thus changing the covalence of B-O bond accordingly, resulting in a lattice defect formation. These defects cause the increased amount of oxygen adsorption and high concentration of oxygen vacancies, leading to a promoted oxygen fluidity in the crystal structure [98–100]. Therefore, perovskites are extensively applied in DRM reaction to enhance the coke resistance of Ni catalysts.

Various elements have been added into $LaNiO_3$ to replace A-site or B-site ions [101–104]. For example, Sr was doped in the perovskite structure to partially substitute A-site La ions to tune the cell dimension and oxygen states. The lattice distortions generated high lattice oxygen mobility, activating C-H bond in CH_4 and adsorbing CO_2 molecules to form $La_2O_2CO_3$ [104]. For B-site replacement as presented in Table 2, Cu partially substituted Ni ions to enhance the mobility of lattice oxygen species, leading to a high conversion of CH_4 but a low catalytic stability because agglomeration of Ni particle took place with a weak MSI. On the contrary, Fe-substituted $LaSrNiFeO_3$ catalyst exhibited a long-term stability in DRM reaction due to the abundance of lattice oxygen and strong MSI [104]. The modification effect of Fe is elucidated in another work [105]. When Fe was doped into $LaNiO_3$ structure, Fe could be converted to FeO and Fe_3O_4 by CO_2 and Fe_3O_4 reacted with La_2O_3 to form $LaFeO_{3-\delta}$, which distorted the lattice structure and produced oxygen vacancies via compensation of the low valency of Fe ions. To modify the A-site of $LaNiFeO_3$, Ce can be added to partially replace the La to introduce more oxygen vacancies by both activating the B-site ions and reversibly shuttling between Ce^{3+} and Ce^{4+}. In detail, unlike Sr^{2+} with a lower valency than La^{3+}, Ce^{3+} was not possible to directly provide oxygen vacancies when doped into the perovskite structure. But according to the TPR profiles as Figure 4 below, the reduction peak of Ni(Fe) ions shifted to lower temperatures with the increase of Ce amount, reflecting an improved reducibility and more oxygen vacancies indirectly offered by Ce. On the other hand, due to the local redox fluctuations of Ce ions, the regeneration of transition metals may be facilitated with the promoted migration inside/outside the perovskite structure. Therefore,

more oxygen vacancies brought by Ce enhanced the oxygen mobility and backfilling of lattice oxygen and promoted the adsorption and activation of CO_2 to CO and oxygen atoms which in turn replenished the oxygen vacancies (seen in Table 2) [106]. As for the B-site of $LaNiFeO_3$, in another study, Co was doped into $LaNiFeO_3$ to improve the oxygen mobility due to the spin state, multivalent property and oxygen affinity. When the molar ratio of Co equaled to 0.1 and 0.3, the modified perovskite structure presented a structural stability and high conversions [101].

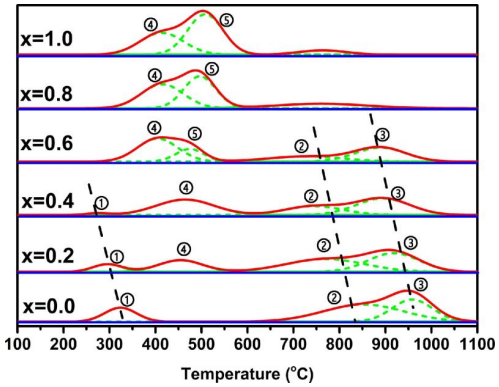

Figure 4. TPR profiles of fresh $La_{1-x}Ce_xNi_{0.5}Fe_{0.5}O_3$ with different x values. Reproduced with permission from reference [106].

Besides $LaNiO_3$ structure, $LaAlO_3$ perovskite catalysts are proved to be more resistant to coke formation than α-Al_2O_3 due to the higher thermal stability and more oxygen vacancies [107]. Two possible mechanisms were illustrated in Figure 5 below, which differed in the location of oxygen vacancies and NiO in the perovskite. When oxygen ions of NiO happened to be in the oxygen vacancies, two electrons of H_2 were released to reduce Ni ions to form metallic Ni and produce H_2O by reacting with O^{2-}, enhancing the dispersion of Ni particles on the surface. When oxygen ions were located adjacent to the oxygen vacancies, H_2 would be heterolytically dissociate into H^+ and H^-. The later adsorbed on the surface of acidic support while the former combined with O^{2-} to produce water. In this case, the reduction of NiO was not preferred and the metal dispersion became poor. These two mechanisms reflected the promotional effect of oxygen vacancies on the migration of lattice oxygen of NiO and coke removal at the perovskite interface.

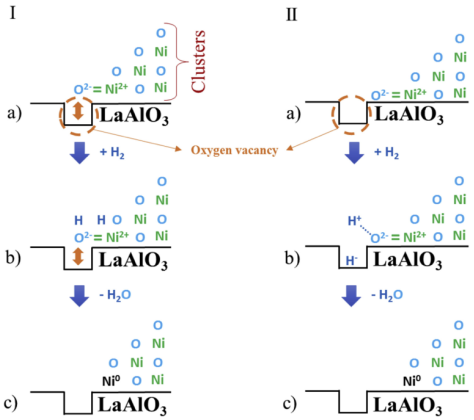

Figure 5. Scheme of the reduction/activation mechanism of the Ni catalyst supported on $LaAlO_3$ catalysts. (**I**)—Terminal oxygen ion of the NiO clusters located on the surface oxygen vacancy. (**II**)—Terminal oxygen ion of the NiO clusters located adjacent to the surface oxygen vacancy. Reproduced with permission from reference [107].

Table 2. A summary of oxygen defects effects on the catalytic performances of Ni-based catalysts for DRM reaction.

Catalyst	Preparation Method	Reaction Condition	Methane Conversion	CO_2 Conversion	Carbon Formation	Comments	Ref.
Ni–CaO–ZrO_2	Co-precipitation method	700 °C; CH_4/CO_2 = 1	73% for CH_4 after 35 h	83% for CO_2 after 35 h	NA	The lattice oxygen of ZrO_2 reacted with CH_x to form CO and H_2 and regenerated the Ni active sites.	[59]
$NiRhCe_2Zr_{1.51}$	Pseudo sol–gel method	700 °C; CH_4/CO_2 = 7:3	16% for CH_4 after 25 h	37.5% for CO_2 after 25 h	4–10 $mg_c/100\ mg_{cat}$	ZrO_2 and CeO_2 formed a cubic phase of $Ce_xZr_{1-x}O_2$, generating more oxygen vacancies and higher oxygen storage capacities than tetragonal phase.	[81]
Ni/CeO_2–ZrO_2	Co-precipitation/molten salt synthesis	750 °C; CH_4/CO_2 = 1	2.56 mmol/(m^2·h)	NA	3.75×10^{-6} $mg_{coke}/(m^2 \cdot h)$	With the increase of Ni concentration, oxygen vacancies increased accordingly.	[82]
PdO–NiO/Y_2O_3	Wet impregnation method	700 °C; $CH_4/CO_2/O_2$ = 2/1/1	91.11% for CH_4 after 24 h	44.98% for CO_2 after 24 h	16.8 $mg/g_{cat}/h$	α-oxygen was found on the surface of Y_2O_3 to activate CH_4 and remove the carbon.	[83]
Ni-SDL (Sr doped La)	Wet impregnation method	600 °C; CH_4/CO_2 = 1	78% for CH_4 after 10 h	60% for CO_2 after 10 h	50 $mg/g_{cat}/h$	The addition of small amount of Sr could enhance the surface oxygen species mobility.	[84]
$Ce_{0.70}La_{0.20}Ni_{0.10}O_{2-\delta}$	Combustion synthesis	750 °C; CH_4/CO_2 = 1	71% for CH_4 after 50 h	83% for CO_2 after 50 h	n.d.	The lattice of CeO_2 expanded due to the partial dissolution of La^{3+} into the lattice structure to generate oxygen vacancies.	[85]
Ni-ZrO_2@SiO_2	Microemulsion method	800 °C; CH_4/CO_2 = 1	90.5% for CH_4 after 240 h	93.2% for CO_2 after 240 h	n.d.	More abundant active oxygen provided by ZrO_2 easily accessed to the carbon species and oxidized the coke to form CO.	[89]
Ni/ZrO_2	Deposition-precipitation method	700 °C; CH_4/CO_2 = 1	52% for CH_4 after 300 min	59% for CO_2 after 300 min	26.7%	The optimal ratio of surface adsorbed oxygen to lattice oxygen was achieved under H_2 treatment.	[90]
$La(Co_xNi_{1-x})_{0.5}Fe_{0.5}O_3$	Sol-gel self-combustion method	750 °C; CH_4/CO_2 = 1	70% for CH_4 after 30 h	80% for CO_2 after 30 h	<3 mg_c/g_{cat}	Co was doped into $LaNiFeO_3$ to improve the oxygen mobility due to the spin state, multivalent property and oxygen affinity of Co.	[102]
$La_{0.8}Sr_{0.2}Ni_{0.8}Cu_{0.2}O_3$	Sol-gel method	600–800 °C; CH_4/CO_2 = 1	80% for CH_4 after 24 h	80% for CO_2 after 24 h	70 $mg/g_{cat}/h$	Partial substitution by Sr and Cu generated higher lattice oxygen mobility.	[105]
$La_{1-x}Ce_xNi_{0.5}Fe_{0.5}O_3$	Sol-gel self-combustion method	750 °C; CH_4/CO_2 = 1	62% for CH_4 after 25 h	72% for CO_2 after 25 h	NA	More oxygen vacancies brought by Ce enhanced the oxygen mobility and backfilling of lattice oxygen.	[107]

In a word, partial substitution of A-site and B-site can generate oxygen vacancies by lattice distortion or redox property, which promotes the lattice oxygen mobility and adsorption of CO_2 to form CO and oxygen atoms. Carbon species derived from the methane activation can be removed by the oxygen atoms, presenting the potential of substituted perovskites as a coke scavenger in the DRM reaction.

For the utilization of oxygen defects, rare earth metal oxides, transition metal oxides and perovskites could be adopted as the supports or promoters which generated oxygen vacancies, surface oxygen or lattice oxygen species, facilitating the mobility of oxygen and oxidizing the coke in time.

4. Interfacial Engineering

Either the metal-metal synergy or metal-support interaction affects the electron density, surface composition and metal dispersion, thus determining the activation of reactants anti-deactivation properties of Ni catalysts [108,109]. In the following, two strategies of interfacial engineering will be discussed in detail, namely Ni-metal alloy formation and Ni–support interaction.

4.1. Ni-Metal Alloy Formation

Bimetallic Ni catalysts enjoy the benefits of synergetic effects between Ni and another metal, such as oxygen affinity, redox cycle, alleviated agglomeration, produced reducibility, dilution effect [109–115]. For example, Cu can modify the Ni environments and prevent carbon formation [116]. Co can inhibit sintering of Ni by formation NiCo alloy and enhance the resistance to oxidation [117]. Nobel metals can improve the Ni dispersion on the surface of the support and increase the tendency of CH oxygenation instead of dehydrogenation [118,119]. The following part will cover the effects of Ni alloys with different groups of metals on the physicochemical properties and catalytic performances of Ni-based catalysts in DRM reaction.

4.1.1. Alloy of Ni and Noble Metals

When noble metals are added to Ni catalysts, the reducibility of Ni is enhanced due to the spillover of H_2 on the surface of noble metals. In the presence of Pt, the reduction temperatures of Ni-Pt alloy shifted to lower regions in the TPR profiles. This was due to the ready adsorption of H_2 molecules on the Pt surface and dissociated into H species which subsequently reduced NiO to form metallic Ni [120]. Besides the promotional effect on the reducibility of Ni ions, noble metals can also alleviate the oxidation of Ni by forming alloys. It is well known that a layer of Ni^{2+} covering the metallic Ni particles reduces the active sites, thus leading to a poor activation of CH_4. Due to the resistance to oxidation under atmospheric or pressurized conditions, noble metals prevent Ni metals from being oxidized when forming alloys [121]. Moreover, Ni dispersion can be enhanced due to the dilution effect of noble metals when forming alloy with them. The resulting small particles contributed to the enhanced coke resistance in DRM reaction [113].

A mechanistic study was to explore the surface composition and reconstruction of Ni and Pt under oxidative environment as shown in Figure 6. When heating a layer of Pt atoms covering Ni bulk, Pt atoms would form a Ni-Pt alloy on the surface. Under oxidative treatment, segregation of Ni from the alloy was observed and the Ni-rich surface was exposed to outside to form O/Ni-Pt-Pt structure. Similarly, when a layer of Ni atoms covered Pt bulk, Ni atoms would diffuse into the sublayers to form a stable Pt-Ni-Pt structure upon being heated. When treated with oxidative atmospheres, Ni again segregated to the surface to form the same O/Ni-Pt-Pt structure. By using EXAFS to characterize the Pt coated Ni catalysts and analyze the coordination number of Pt-Ni and Pt-Pt, an increased value of N (Pt-Ni) and decreased value of N (Pt-Pt) reflected the migration of Pt to sublayers and Ni to the surface, transforming the Pt monolayer to a core-shell structure with Ni as the core and Ni-Pt alloy as the shell. This resulting structure facilitated the oxidation of CH and carbon removal (seen in Table 3) [119]. Moreover, recent operando studies suggested that the formation of PtNi alloys could promote the

formation of Ni oxide surface clusters, which related to the strong MSI effect, thus leading to a catalytic performance enhancement [122,123].

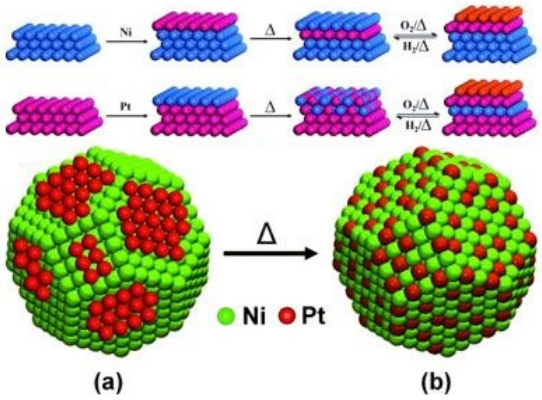

Figure 6. (**a**) Surface restructuring of Ni/Pt bimetallic systems induced by temperature and adsorbates. (**b**) Evolution of the surface structure of the Ni/Pt bimetallic NPs upon thermal treatment. Reproduced with permission from reference [119].

Preparation methods may affect the surface composition. When co-impregnation was applied to prepare Ni-Pd/Al_2O_3 catalyst, a uniform Ni-Pd alloy was formed due to the strong interaction between two metals. When sequential impregnation was utilized, segregation of Pd atoms was observed because of the weak interaction. In this case, Pd atoms preferred to locate on the surface instead of diffusing into the sublayers [124].

4.1.2. Alloy of Ni and Transition Metals

Similar with noble metals, transition metals can enhance the anti-sintering and anti-coking properties of Ni catalysts by forming alloys [39,77,125–129]. But the driver force may differ from that of noble metals.

After the addition of Co, Ni-Co alloys exhibited an improved affinity for oxygen but a stronger resistance to oxidation than Co alone [130]. First principle calculations showed that Co was very sensitive to oxygen which was proved by the experimental results that when Co loading was below 9 wt% on Al_2O_3, the Co metals suffered from oxidation, thus losing the active sites and deactivating DRM reaction [131]. However, when Ni-Co alloy was formed, due to the synergy between two metals, both the oxidation of metals and carbon formation were inhibited due to the adsorption of CO_2. At 800 °C, only 1.7 wt% of carbon deposits were produced after 100 h DRM reaction [130,132]. One possible explanation for the inhibition effect of Co on oxidation is demonstrated by Gao et al. [133] in the XPS study of reduced Ni-Co/SiO_2, whereby the shift of the binding energies of Ni and Co reflected the donation of electrons from Co to Ni, increasing the electron density of Ni and prevented Ni from being oxidized. Meanwhile, metal sintering was also impeded. As for the anti-coking ability, DFT calculations showed that the activation of CH_4 on Ni clusters produced mainly CH_3 and H species; while for Ni-Co alloy, due to the high affinity of Co for oxygen, CH_4 reacted with oxygen atoms to form CH_3 and OH species, which removed surface carbon deposits more readily (shown in Table 3) [134].

Compared with Co, the addition of Fe mostly reduces the carbon deposits via redox cycle. In the Ni-Fe/$MgAl_2O_4$ catalyst, after pulse injection of CO_2, Ni-Fe decomposed to form metallic Ni and Fe. Different from stable Ni phase, Fe was easily to be oxidized to FeO_x. Following the Mars–van Krevelen (MvK) mechanism, carbon species on the surface of Ni were oxidized by FeO_x to form CO and Fe [135]. Likewise, in another study, dealloying and realloying process took place during the DRM reaction. In detail as shown in Table 3, CO_2 adsorbed on the Ni-Fe alloy oxidized the Fe to form FeO, which reacted with the carbon derived from the CH_4 decomposition to form CO and regenerate metallic Fe. The redox cycle of Fe/Fe^{2+} was crucial in inhibiting the carbon formation [136].

As another transition metal, Cu has been proved effective in DRM reaction when forming alloy with Ni. On one hand, Cu alleviated the metal sintering after 30 h reaction; on the other hand, with a molar ratio of Cu:Ni equaling to 1:3, a high conversion of reactants with minimal carbon formation was achieved [137]. A possible mechanism was elucidated by DFT calculation that O(OH) species preferred to adsorb on the CuNi (111) phase, which promoted the elimination of carbon deposits. Besides the DFT calculations, experimental evidence is expected [26].

As for the Cu amount, it was found that by increasing the concentration of Cu, methane activation may be inhibited since Ni active sites were covered by Cu which exhibited slower dissociation kinetics than Ni. As shown in Table 3, this competitive adsorption can be minimized by a careful control of the amount of Cu added in the Ni catalysts [137].

4.2. Ni-Support Interaction

Metal-support interaction (MSI) influences the metal size, dispersion, surface area and reducibility of Ni-catalysts, in turn determining the reactivity and stability in DRM reaction [26,30]. MSI can be turned by the support materials and promoters/dopants. For example, though silica is an inert support, by adopting a modified prepared method, a stable Ni phyllosilicate structure can be formed which enhances the MSI and controls the size and dispersion of Ni [29]. Ca as a promoter promotes the interaction between Ni and Al_2O_3, thus impeding the metal sintering and improving the dispersion of Ni [138]. However, a too strong MSI may exert a negative impact on the metal surface area since a high reduction temperature is needed [30].

When CeO_2 was used as the support for Ni, strong MSI was formed, which facilitated the dissociation of methane in DRM reaction [65,67]. By DFT calculations, the activation barrier for Ni alone was 0.9 eV while for Ni-CeO_{2-x}, the value dropped to 0.15 eV only. It is widely known that the rate determining step for DRM reaction is the activation of C-H bond in CH_4 molecules [139], therefore, a lower value of activation energy enhanced the reaction rate and energy efficiency. After 80 h reaction at 450 °C, the conversion was 12%, close to the equilibrium value at this condition. As for the reaction pathway, once the first H was released from CH_4, the following transformation of CH_x species proceeded very quickly. The carbon species was oxidized by the O adatoms of CO_2 to form CO, and H desorbed the surface in the form of H_2 and H_2O. Interestingly, the non-defective CeO_2 exhibited no signs of CO_2 activation. Only when the Ni^{2+} and Ce^{4+} were reduced by the decomposition products of CH_4 to form metallic Ni and Ce^{3+}, could the CO_2 reacted with oxygen vacancies and H adatoms produced by methane activation to form CO. This was proved by the decreased amount of Ce^{3+} exposed to CH_4 and CO_2 atmospheres compared with CH_4 alone according to Ce 4d XPS results as shown in Figure 7 below. In summary as presented in Table 3, Ni and O atoms cooperatively adsorbed the CH_4 molecules due to the Ni-Ce solid solution formation, where a strong MSI tuned the electronic or chemical properties of Ni, thus enhancing the activation of methane by Ni metals and inhibiting the carbon formation proved by the lack of C or NiC_x peaks as below [65].

Similarly, in another work, under a small Ni coverage, Ni and O atoms collaboratively activated the C-H bond in CH_4, leading to a good conversion at low reaction temperature 377 °C. Due to the strong MSI and electrons transfer from Ni to CeO_2, Ni^{2+} and Ce^{3+} formed, generating the most stable site Ni^{2+}@O-hollow. Ni^{2+} was the only Ni species either before or after the adsorption of CH_4 at room temperatures. When the coverage of Ni increased to 0.5 ML, NiC_x species appeared on the surface; when the Ni coverage was below 0.2 ML, the small Ni atoms or particles contacted closely with the CeO_2 support, resulting in a much lower activation energy of CH_4 than that with a Ni coverage of 0.5 ML. A small loading of Ni formed small particles, which experienced large electronic perturbations from CeO_2. These small Ni particles and O atoms in CeO_2 promoted the activation of CH_4 in a cooperative way. When Ni^{2+}/CeO_2 was transformed to Ni^0/CeO_{2-x} by reacting with C species from CH_4 decomposition, CO and oxygen vacancies were generated [67,140,141]; the oxygen vacancies formed on the reduced CeO_{2-x} facilitated the adsorption and activation of CO_2, thus leading to an enhanced conversion and stability in DRM reaction [67].

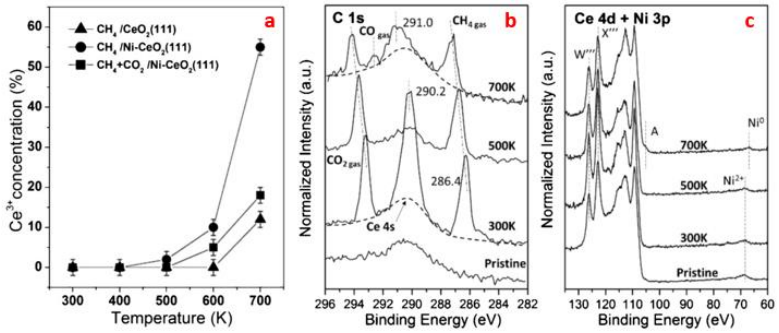

Figure 7. (**a**) Ce^{3+} concentration measured in XPS as a function of temperature under reaction conditions (i.e., exposure to 100 mTorr of methane or a mixture of 100 mTorr of methane and 100 mTorr of CO_2). (**b**,**c**) C 1s and Ce 4d + Ni 3p spectra of the Ni-CeO_2(111) ($\theta_{Ni} \approx 0.1$ ML) surface under 100 mTorr CH_4 + 100 mTorr of CO_2 at 27, 227, and 427 °C. Reproduced with permission from reference [65].

In certain situations, however, strong MSI may not be a benefit. As shown in Table 3, when a layer of CeO_2 covered the Ni-Co alloys, the promotional effect of Co on the enhanced MSI was cancelled off by the reduction of active sites exposed to the reactants [63]. Similar findings were shown presented for the Ni/TiO_2. Despite the strong MSI, the surface free energy may be reduced due to the coverage of Ni active sites by the migration of TiO_x species over the surface.

In addition to CeO_2, owing to the strong basicity of MgO, a strong MSI between Ni and MgO derived from the solid solution probably enhance the anti-coking property [142,143]. However, the surface and under-coordinated Ni still exhibited a sensitivity to coke formation [144]. $MgAl_2O_4$ spinel structure may be a promising candidate to produce a highly dispersed Ni particles due to the strong MSI; together with the basicity of the support, CO_2 adsorption will be promoted, and carbon deposition will be alleviated (seen in Table 3) [145]. But an extraordinarily strong MSI may bring a high reduction temperature, possibly leading to the metal sintering. To further modify the dispersion of Ni, Co was added to the Ni/$MgAl_2O_4$ to slow the reduction of Ni and generate a small and uniform Ni particle, resulting in an enhanced DRM activity [146].

Besides the rare earth metal oxides, alkali earth metal oxides and transition metal oxides, SiO_2 as a support can also form a stable structure with Ni species with a modified preparation method [147,148]. With the addition of NH_3 to control the pH, Ni phyllosilicate formed between the Ni and SiO_2 under thermal treatment of Ni precursors. Upon decomposition of the phyllosilicate, highly dispersed Ni particles interacted strongly with the SiO_2, achieving a high and stable conversion of CH_4 (74%) and CO_2 (82%) over 50 h at 700 °C as seen in Table 3 [149].

In addition to the ammonia-assisted method, thermal treatment also benefited the Ni phyllosilicate formation. Compared with air calcination or H_2 treatment, a sequential calcination method was advantageous in terms of the size and MSI of Ni/SiO_2 catalysts. In detail, the first step of H_2 calcination at 400 °C scavenged oxygen radicals produced from the nitrate decomposition, reducing the Ni particle size and enhance the dispersion. The subsequent air calcination at 700 °C strengthened the MSI by forming the Ni phyllosilicate, anchoring Ni particles and preventing the sintering. As presented in Table 3, the Ni/SiO_2 catalyst prepared with the facile modified incipient wetness impregnation method exhibited an outstanding catalytic performance (80% for CH_4 and 85% for CO_2) with little sintering and no coke formation after 100 h DRM reaction [150].

In a word, by adjusting the Ni-metal interface and Ni-support interaction, the physicochemical properties of Ni catalysts can be improved due to the synergy between Ni and dopant metals and the electronic and chemical perturbation by the support. In turn, catalytic performances and anti-deactivation abilities in DRM reaction can be enhanced by introducing oxygen vacancies, surface basicity, oxygen affinity, redox cycle, low activation barrier, steric hindrance, and electron transfer upon interfacial engineering in Ni-based catalysts.

Table 3. A summary of interfacial engineering effects on the catalytic performances of Ni-based catalysts for DRM reaction.

Catalyst	Preparation Method	Reaction Condition	Methane Conversion	CO_2 Conversion	Carbon Formation	Comments	Ref.
$NiCo/CeO_2$	Incipient wetness impregnation method	700 °C; $CH_4/CO_2 = 1$	64% for CH_4 after 300 min	69% for CO_2 after 300 min	11.5%	When a layer of CeO_2 covered the Ni-Co alloys, the promotional effect of Co on the enhanced MSI was cancelled off.	[63]
Ni/CeO_2	NA	450 °C; $CH_4/CO_2 = 1$	10^{-7} torr CH_4 after 80 h	10^{-7} torr CO_2 after 80 h	NA	Ni and O atoms cooperatively adsorbed the CH_4 molecules due to the Ni-Ce solid solution formation.	[65]
Ni/TiO_2	Impregnation method	790 °C; $CH_4/CO_2 = 1$	41% for CH_4 initially	67% for CO_2 initially	8.0×10^{-4} g_C/g_{cat}	The surface free energy may be reduced due to the coverage of Ni active sites by the migration of TiO_x species.	[108]
$NiPt/Al_2O_3$	NA	700 °C; $CH_4/CO_2 = 1$	85.8% for CH_4 after 18 h	91.2% for CO_2 after 18 h	0.1 $mol_C/mol_{surface\ metal}/h$	Pt monolayer in a core-shell structure with Ni facilitated the oxidation of CH and carbon removal.	[119]
$NiCo/MgO\text{-}ZrO_2$	Co-precipitation and impregnation method	600 °C; $CH_4/CO_2 = 1$	6.6 $mol\cdot(g\cdot atom\cdot NiCo_{surface}\cdot s)^{-1}$	NA	NA	For Ni-Co alloy, due to the high affinity of Co for oxygen, CH_4 reacted with oxygen atoms to form CH_3 and OH species.	[134]
$Fe\text{-}Ni/MgAl_2O_4$	Co-precipitation and incipient wetness impregnation method	750 °C; $CH_4/CO_2 = 1$	0.13 $mol_{CH4}\ s^{-1}\ mol_{Ni}{}^{-1}$ after third cycle	NA	5.02 $mol_{CO}\ mol_{Ni+Fe}{}^{-1}$	Carbon species on the surface of Ni were oxidized by FeO_x to form CO and Fe.	[135]
$Fe\text{-}Ni/MgAl_2O_4$	Co-precipitation and incipient wetness impregnation method	750 °C; $CH_4/CO_2 = 1$	NA	NA	NA	The redox cycle of Fe/Fe^{2+} was crucial in inhibiting the carbon formation.	[136]
$Cu\text{–}Ni/SiO_2$	Hydrothermal process	700 °C; $CH_4/CO_2 = 1$	70% for CH_4 after 30 h	NA	3%	When Cu formed alloy with Ni, the metal sintering and carbon formation were alleviated.	[137]
Ca-promoted $Ni/\alpha\text{-}Al_2O_3$	Wetness co-impregnation method	800 °C; $CH_4/CO_2 = 1$	84.8% for CH_4 after 240 min	85.5% for CO_2 after 240 min	24.9 $mg/g_{cat}/h$	Ca promoted the interaction between Ni and Al_2O_3, thus impeding the metal sintering and improving the dispersion of Ni.	[138]
$AuNi/MgAl_2O_4$	Sol preparation method	650 °C; CH_4/CO_2 = 69:30	20% for CH_4 after 1000 min	48% for CO_2 after 1000 min	3 mg	$MgAl_2O_4$ spinel structure increased the basicity of the support, so CO_2 adsorption will be promoted, and carbon deposition will be alleviated	[145]
Ni@Ni embedded SiO_2	Self-templating method	700 °C; $CH_4/CO_2 = 1$	74% for CH_4 after 50 h	82% for CO_2 after 50 h	n.d.	Upon decomposition of the phyllosilicate, highly dispersed Ni particles interacted strongly with the SiO_2.	[149]
Ni/SiO_2	Incipient wetness impregnation method	700 °C; $CH_4/CO_2 = 1$	80% for CH_4 after 100 h	85% for CO_2 after 100 h	n.d.	Sequential H_2-air calcination enhanced Ni dispersion and MSI with SiO_2.	[150]

5. Structural Optimization

A small particle size can enhance the activity of Ni-based catalysts [151]. To alleviate the Ni sintering at high temperatures during DRM reactions, optimizations have been made on the structure of supports, such as porous materials which enhance the surface area and providing the anchoring points for metal active sites [30,31]. Moreover, hierarchical designs of the catalyst including core-shell, yolk-shell, embedded and hollow structures, sterically hinder the migration of Ni and prevent the agglomeration [27,30].

5.1. Porous Supports

High porosity of carbon materials inhibits the movement of metal particles and enhances the dispersion on the carbon support. Also, porous carbon materials can be prepared into various physical forms, such as pellets, cloth, and fiber [30]. Li et al. [152] synthesized porous carbon from renewable hydrochar as the precursor and successfully anchored Ni^{2+} ions on the surface, leading to highly dispersed Ni nanoparticles with the diameter of less than 8 nm. Methane conversions reached 52% and 70% for 700 °C and 800 °C pretreated catalyst respectively.

In addition to porous carbon materials, silica with high porosities and ordered structures is widely used to control the particle size and enhance the metal dispersion by confining metal particles in the pores (seen in Table 4) [153–158]. SBA-15 with silanol groups on its surface was able to trap the Ni ions by bonding with amine groups of polyethylenimine (PEI) in the Ni-PEI complexes (Figure 8). Little sintering took place due to the confinement effect of SBA-15 with ordered channels, leading to a high stability over 40 h of reaction [155]. When ethylene glycol (EG) was used as the solvent, Ni-EG complexes were pumped into the pores of SBA-15 by capillary force, hindering the migration of Ni during the drying and calcination process [154].

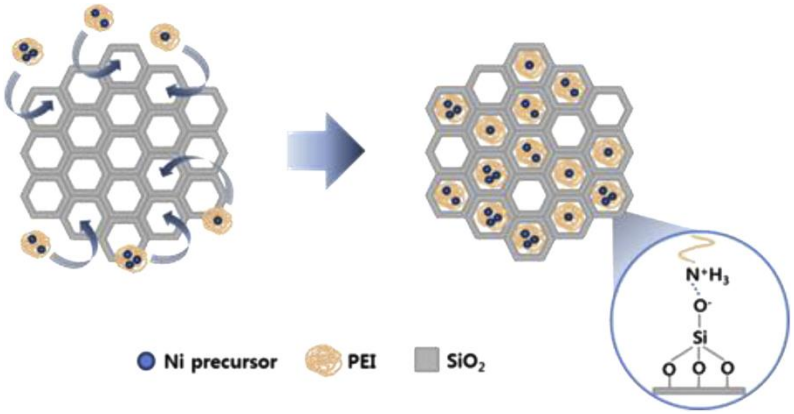

Figure 8. Schematic diagram of PEI-aided route. Reproduced with permission from reference [155].

As shown in Table 4, besides Ni monometallic catalysts, bimetallic Ni-Co supported on SBA-15 maintained the activity over 50 h. The small particle size (4–5 nm) and high metal dispersions (17–20%) were achieved by the confinement effect of ordered channel of SBA-15 [159]. Perovskite structures $LaNiO_3$ were also impregnated into the mesoporous SBA-15 supports. With the help of the stable structures, the conversions were kept stable over 60 h without agglomeration of Ni particles [160].

Compared with SBA-15, MCM-41 and KIT-6 supported Ni catalysts exhibited lower conversions and higher carbon depositions in DRM reaction. For KIT-6, the micropores were occupied by Ni particles so that the pathways of reactants were blocked despite the high Ni dispersion [157]. For MCM-41, it suffered poorer structural stability than SBA-15 especially when TiO_x and MnO_x hindered the channels for reactants to pass through and the amorphous form of silica was transformed into crystals [161,162].

To enhance the diffusion efficiency and thermal stability, as shown in Table 4, hexagonal mesoporous silica (HMS) with thicker pore walls and more interconnected channels was applied as the support of Ni to improve the metal dispersion and inhibit sintering by forming Si-O-Ni bonds, leading to a stable conversion over 100 h at 700 °C [158].

For other mesoporous silica supports, one way to enhance the metal dispersion on porous silica supports is to utilize a novel method (seen in Table 4). Colloidal approach was applied by converting Ni-silicide colloids into highly dispersed Ni nanoensembles supported on porous silica under thermal treatment, achieving a 60% higher syngas yields [163]. Polyols precursors were treated under inert atmospheres and decomposed to produce carbon residues, protecting Ni particles from migrating from internal pores to external surfaces. The near-equilibrium conversions at 750 °C resulted from the well-dispersed Ni particles inside the mesoporous channels exposed completely to the reactants [164].

In addition to the colloidal and polyols approaches, ligand-assisted incipient wetness impregnation (IWI) method is applied to control the size and MSI (presented in Table 4). Similar with PEI and EG forming complexes with Ni ions on SBA-15 supports, a combination of oleic acid (OA) and oleylamine (OAm) were used as co-ligands to protect Ni from agglomeration by ligand bonds between Ni ions and amine groups of OAm and hydrogen bonds between carboxylic groups of OA and silanol groups of mesoporous silica. Together with the steric hindrance of the hydrocarbon chain network, a high dispersion of Ni particles and strong MSI were achieved, leading to a stable activity in DRM reaction [165]. Moreover, this method proved effective for reducing the size bimetallic Ni-Co to 3.1 nm averagely, resulting in a high conversion of methane and CO_2 over 30 h at 700 °C [133]. Furthermore, in a systematic study of the amine effect, the organic amines with a long hydrocarbon chain and high concentration produced a small size of Ni and a high dispersion as well as a strong MSI [166].

Compared with inert materials like carbon and silica, alkali earth metal oxides, rare earth metal oxides and alumina presented both a porous structure and a surface modification effect [167–170]. NiO-MgO-Al_2O_3 mesoporous frameworks provided more active centers for the reactants to be activated and converted to syngas products. Ni particles were anchored within the pores to alleviate the sintering effect and prolong the lifetime in the reaction; with the basic promoters, carbon removal was facilitated due to the adsorption of CO_2 which was dissociated into CO and oxygen radicals (seen in Table 4) [167]. In another example as shown in Figure 9, mesoporous NiO-CeO_2-Al_2O_3 materials was prepared by evaporation-induced self-assembly method with the introduction of CeO_2 into Ni/Al_2O_3. The excellent thermal stability of this mesoporous structures (preserved over 80 h at 700 °C) effectively protected Ni from sintering. Also, the redox property of CeO_2 oxidized carbon deposits to help maintain the exposure of active sites to reactants during the reaction [171].

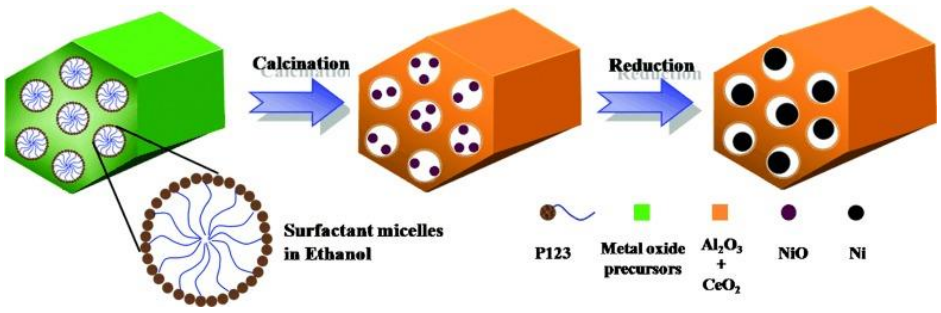

Figure 9. Schematic illustration of the NiCeAl (R) preparation. Reproduced with permission from reference [171].

In a word, various porous materials such as carbon, silica and alumina provide accommodations for Ni nanoparticles to be protected from migrating from internal pores to external surfaces of the supports. Organic ligands, novel methods and promoters are utilized to further enhance the anti-sintering and anti-coking capabilities, leading to a high conversion of methane and CO_2 and long-term stability.

5.2. Hierarchical Designs

Besides the rational design of the porous supports to enhance the surface area and confine the metal nanoparticles inside the pores or channels, architecture optimizations of the catalysts have become an effective method to improve the sintering and coking resistance. Owing to the uniform microporosity, high thermal stability and unique shape selectivity, zeolites draw attentions in stabilizing Ni particles and prevent the sintering during DRM reaction [172,173]. Moreover, other smart designs emerge in recent years, such as core-shell structures. With the first design of "nanoreactor" Pt@CoO core-shell nanostructures, various nanocomposites containing metal and metal oxides protected by silica shells are developed in recent years, including core-shell, yolk-shell, hollow and embedded structures, to partially separate metal particles from each other and enhance the dispersion [30,174–182].

Ni@SiO_2 core-shell catalysts with Ni as the core and SiO_2 as the shell exhibited a strong resistance towards filamentous carbon deposition (shown in Table 4). However, amorphous carbon still formed within the nanocavities between the core and shell. Minimizing the nanocavities was recommended to modify the structure and improve the coke resistance [183].

To enhance the catalytic performance, a thick SiO_2 shell was formed to transform the core-shell structure to yolk-shell structures with Ni as the core surrounded by Ni nanoparticles embedded in the SiO_2 shell (Figure 10). With a 11.2 nm of thickness, this unique structure exhibited an enhanced conversion and stability in DRM reaction with the help of strong MSI and small satellite Ni particles [184]. However, the turnover frequency (TOF) can be increased by tuning surface area and Ni exposure. Instead of using micro-emulsion method, a self-templating method was utilized to successfully prepared a yolk-shell Ni@SiO_2 catalyst, increasing the TOF by 4.5 times of the previous one (shown in Table 4) [149].

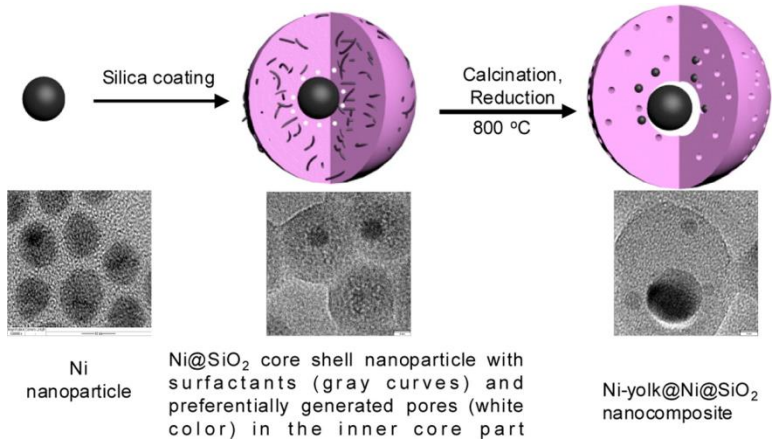

Figure 10. Schematic illustration of the formation process of Ni−yolk@Ni@SiO_2 nanocomposite. Reproduced with permission from reference [184].

To further enhance the active surface area and metal loadings, as presented in Table 4, multi-core shell catalysts with multiple Ni cores and a mesoporous SiO_2 shell were synthesized by reversed micelle method. During the reaction, Ni particles migrated into the SiO_2 shell, leading to the formation of uni-nuclear Ni core embedded in the shell [185]. To achieve a better anti-sintering property, a layer of silica was coated on the multiple Ni cores supported on the mesoporous silica as shown in Figure 11. With the protective layer of silica, 5.2 nm of Ni particles with a narrow size distribution were prevented from agglomeration due to the strong MSI and steric hindrance, reaching a high stability over 170 h at 800 °C [186].

To improve the MSI between Ni and SiO_2, Ni phyllosilicate structures were prepared by ammonia evaporation method, which generated highly dispersed Ni nanoparticles with the size of 6 nm supported on silica. With a layer of SiO_2 covering the Ni metals, a good activity was achieved at 600 °C over 24 h because of the enhanced MSI and confinement effect of mesoporous SiO_2 [182].

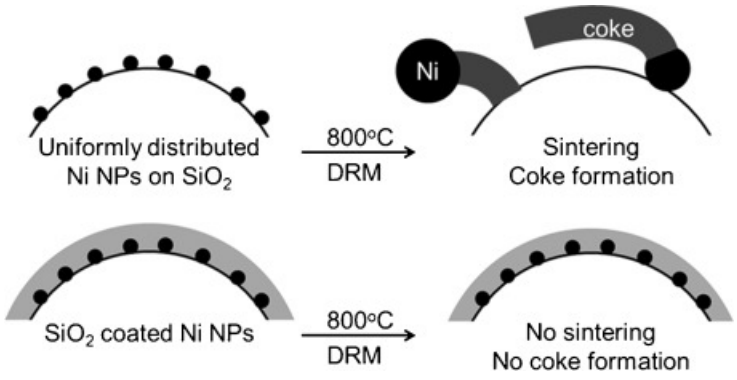

Figure 11. DRM with highly coke-resistant silica-coated nickel nanoparticle catalysts. Reproduced with permission from reference [186].

As for the controlled synthesis of Ni phyllosilicate, Ni precursors exerted an influence on the size of Ni particles, thus affecting the diffusion speed through the Ni phyllosilicate layer to form a new phyllosilicate species with silicate ions (seen in Table 4). Ni acetylacetonate, among various precursors, reacted with mesoporous silica spheres to form Ni phyllosilicates by hydrothermal method, exhibiting a unique pore structure with the smallest pore volume and pore size. This strong MSI between Ni and the support retarded carbon nanotube formation by anchoring Ni on the silica [147].

Besides the effect of precursors on the size of Ni, as shown in Table 4, modification of the porosity and basicity can further enhance the adsorption and accessibility of reactants. Therefore, Ni-Mg phyllosilicate were synthesized via facile hydrothermal method as shown in Figure 12. By adjusting the duration of treatment, an ideal porosity and basicity could be realized [187]. On one hand, due to the high affinity of MgO for CO_2, more reactants were adsorbed on the surface more easily through a modified pore structure, accelerating the conversion of methane and the removal of carbon deposits. On the other hand, because of the strong MSI between Ni and MgO, metal sintering could be prevented to a large extent. Together with the protective layer of mesoporous silica, this catalyst maintained active for 72 h at 750 °C [188].

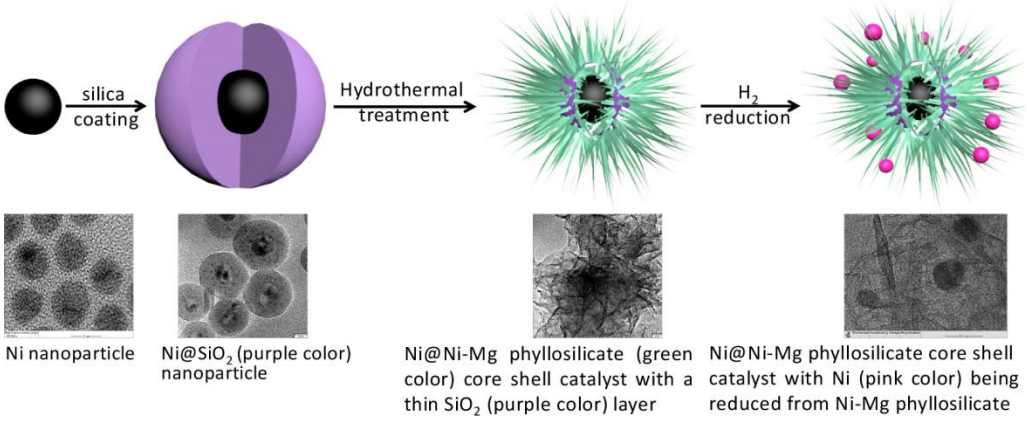

Figure 12. Schematic illustration of the formation process of Ni@Ni–Mg phyllosilicate core–shell catalyst. Reproduced with permission from reference [187].

Likewise, as shown in Table 4, NiMgAl layer double hydroxide was firstly synthesized by hydrothermal method, followed by coating a layer of mesoporous silica (Figure 13). After calcination and reduction, Ni nanoparticles were generated inside the cavity, which were confined by both MgO and silica layer. The synergies between the confinement effect of mesoporous silica and basicity of MgO resulted in an 8 h stable conversion at 750 °C with little carbon deposition [189].

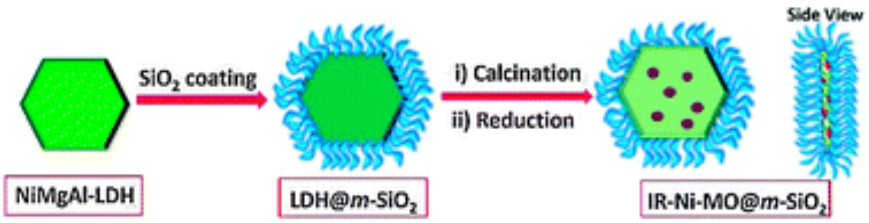

Figure 13. Schematic illustration of the modular catalysts. Reproduced with permission from reference [189].

Besides Ni monometallic catalysts, the core–shell structures can be extended to Ni-based bimetallic catalysts. 12 nm Ni-Cu alloys were successfully synthesized by tuning the precursor concentrations. Being covered by the silica shell, the sintering of alloys could be alleviated, presenting a higher conversion than impregnated samples. Moreover, higher H_2 selectivity could be achieved by the suppression effect on RWGS reaction with the addition of Cu (shown in Table 4) [190].

Ni-Co@silica core-shell structures calcined at 500 °C exhibited poor activities and stabilities. However, as presented in Table 4, when calcined at 800 °C, with the increase of crystallinity of SiO_2 and enhanced MSI, the activity could be maintained stable over 1000 h, reflecting the high thermal stability of the support [191].

In a word, by designing the hierarchical structures of Ni-based catalysts, Ni particle size can be controlled, metal sintering can be alleviated, and coke resistance can be enhanced due to the confinement effect of silica shell and strong MSI derived from the Ni phyllosilicate. By doping another metal (Co, Cu, and Fe) to form alloys with Ni and adding Mg precursors to prepare Ni-Mg phyllosilicates, the activity and stability of the catalysts for DRM reaction can be further enhanced because of the promotional effects, such as the adsorption of CO_2 and suppression of RWGS reaction.

Table 4. A summary of structural optimization effects on the catalytic performances of Ni-based catalysts for DRM reaction.

Catalyst [a)]	Preparation Method	Reaction Condition	Methane Conversion	CO_2 Conversion	Carbon Formation	Comments	Ref.
$NiCo/SiO_2$	Incipient wetness impregnation method	700 °C; CH_4/CO_2 = 1	73% for CH_4 after 30 h	77% for CO_2 after 30 h	n.d.	Homogeneous Ni-Co alloy supported on mesoporous silica was synthesized by oleylamine/oleic acid organic pair.	[133]
NiPhy (Ni phyllosilicate) hollow sphere (HS)	Hydrothermal method	700 °C; CH_4/CO_2 = 1	77.5% for CH_4 after 70 h	86.6% for CO_2 after 70 h	<5%	Ni phyllosilicates exhibited a unique pore structure with the smallest pore volume and pore size.	[147]
Ni yolk@Ni@SiO_2	Self-templating method	700 °C; CH_4/CO_2 = 1	74% for CH_4 after 50 h	82% for CO_2 after 50 h	1.4%	A yolk-shell Ni@SiO_2 catalyst increased the TOF by tuning surface area and Ni exposure	[149]
Ni@C	Wet impregnation method	700 °C; CH_4/CO_2 = 1	68% for CH_4 after 800 min	80% for CO_2 after 800 min	79.3%	Porous carbon anchored Ni^{2+} and enhanced dispersion.	[151]
Ni/SBA-15	Modified impregnation method	750 °C; CH_4/CO_2 = 1	87% for CH_4 after 34 h	92% for CO_2 after 34 h	3.8%	Ni-EG complexes were pumped into the pores of SBA-15 by capillary force, hindering the migration of Ni.	[154]
Ni/SBA-15	Modified impregnation method	750 °C; CH_4/CO_2 = 1	85% for CH_4 after 40 h	88% for CO_2 after 40 h	3.63 mg_c/g_{cat}	Little sintering took place due to the confinement effect of SBA-15 with ordered channels.	[155]
Ni/KIT-6	Impregnation method	750 °C; CH_4/CO_2 = 1	60% for CH_4 after 20 h	78% for CO_2 after 20 h	NA	The micropores were occupied by Ni particles so that the pathways of reactants were blocked despite the high Ni dispersion.	[157]
Ni/HMS	S^0I^0 assembly pathways	700 °C; CH_4/CO_2 = 1	72% for CH_4 after 100 h	84% for CO_2 after 100 h	6.22%	Hexagonal mesoporous silica (HMS) improved the metal dispersion and inhibit sintering by forming Si-O-Ni bonds.	[158]
NiCo/SBA-15	Co-precipitation method	700 °C; CH_4/CO_2 = 1	70% for CH_4 after 50 h	78% for CO_2 after 50 h	n.d.	Small particle size (4–5 nm) and high metal dispersions (17–20%) were achieved by the confinement effect of ordered channel of SBA-15.	[159]
$La_xNi_yO_z$/KIT-6	Sol-gel method	800 °C; CH_4/CO_2 = 1	88% for CH_4 after 60 h	100% for CO_2 after 60 h	3.41%	Perovskite structures $LaNiO_3$ were also impregnated into the mesoporous SBA-15 supports.	[160]
Ni (Si_yO_z)/SiO_2	Colloidal approach	500 °C; CH_4/CO_2 = 1.3	465 mol_{CO}/ h·$mol_{tot.Ni}$	450 mol_{CO2}/ h·$mol_{tot.Ni}$	NA	Colloidal approach was applied by converting Ni-silicide colloids into highly dispersed Ni nanoensembles supported on porous silica.	[163]
Ni/SiO_2	Incipient wetness impregnation method	700 °C; CH_4/CO_2 = 1	70% for CH_4 after 1000 min	72% for CO_2 after 1000 min	n.d.	Co-ligands to protect Ni from agglomeration by ligand and hydrogen bond and steric hindrance.	[165]
Ni/SiO_2	Incipient wetness impregnation method	700 °C; CH_4/CO_2 = 1	70% for CH_4 after 20 h	78% for CO_2 after 20 h	1.8 mg_c/g_{cat} h	With a small size, high dispersion and strong MSI, Ni/SiO_2 prepared with oleylamine showed the most stable catalytic performances.	[166]

Table 4. *Cont.*

Catalyst [a)]	Preparation Method	Reaction Condition	Methane Conversion	CO_2 Conversion	Carbon Formation	Comments	Ref.
NiO–MgO–Al_2O_3	evaporation induced self-assembly strategy	700 °C; CH_4/CO_2 = 1	78% for CH_4 after 100 h	83% for CO_2 after 100 h	7.0%	Ni particles were anchored within the pores to alleviate the sintering effect and basicity of support could enhance CO_2 adsorption and remove coke.	[167]
NiO-CeO_2-Al_2O_3	evaporation induced self-assembly strategy	700 °C; CH_4/CO_2 = 1	78% for CH_4 after 80 h	73% for CO_2 initially	21.5%	The excellent thermal stability of this mesoporous structures protected Ni from sintering and the redox property of CeO_2 oxidized carbon deposits.	[171]
Silica@Ni@Silica	Ammonia evaporation method	600 °C; CH_4/CO_2 = 1	44% for CH_4 after 24 h	54% for CO_2 after 24 h	7.6%	With a layer of SiO_2 covering the Ni metals, a good activity was achieved at 600 °C over 24 h	[180]
Ni@SiO_2	Sol-gel process	750 °C; CH_4/CO_2 = 1	54.1% for CH_4 after 25 h	65.6% for CO_2 after 25 h	1.2%	Strong resistance towards filamentous carbon deposition was exhibited; however, amorphous carbon still formed within the nanocavities	[183]
Ni@SiO_2	Microemulsion method	800 °C; CH_4/CO_2 = 1	90% for CH_4 after 90 h	95% for CO_2 after 90 h	4.8%	With a 11.2 nm of thickness, this unique structure exhibited an enhanced conversion and stability with the strong MSI and small satellite Ni particles.	[184]
Ni@SiO_2	Reverse micelle method	800 °C; CH_4/CO_2 = 1	87% for CH_4 after 100 h	88% for CO_2 after 100 h	NA	Ni particles migrated into the SiO_2 shell, leading to the formation of uni-nuclear Ni core embedded in the shell.	[185]
Silica coated Ni/SiO_2	Microemulsion method	800 °C; CH_4/CO_2 = 1	42.5% for CH_4 after 170 h	56.6% for CO_2 after 170 h	n.d.	To achieve a better anti-sintering property, a layer of silica was coated.	[186]
Ni@Ni-MgPhy	Hydrothermal method	700 °C; CH_4/CO_2 = 1	78% for CH_4 after 95 h	81% for CO_2 after 95 h	4.4% after 20 h	By adjusting the duration of treatment, an ideal porosity and basicity could be realized.	[187]
Ni@Ni-MgPhy	Hydrothermal method	750 °C; CH_4/CO_2 = 1	85% for CH_4 after 72 h	89% for CO_2 after 72 h	n.d.	Strong MSI and the protective layer of mesoporous silica prevented metal sintering.	[188]
NiMgAl-(LDH)@mesoporous-SiO_2	Hydrothermal and sol-gel method	750 °C; CH_4/CO_2 = 1	79% for CH_4 after 8 h	88% for CH_4 after 8 h	2.5%	Ni nanoparticles were generated inside the cavity, which were confined by both MgO and silica layer.	[189]
Cu–Ni@SiO_2	Microemulsion method	700 °C; CH_4/CO_2 = 1	75% for CH_4 after 16 h	NA	NA	Being covered by the silica shell, the sintering of alloys could be alleviated.	[190]
NiCo@SiO_2	Microemulsion method	800 °C; CH_4/CO_2 = 1	90% for CH_4 after 1000 h	90% for CO_2 after 1000 h	n.d. after 150 h	With the increase of crystallinity of SiO_2 and enhanced MSI, the activity could be maintained stable.	[191]

[a)] AC: active carbon; HMS: Hexagonal mesoporous silica; LDH: layered double hydroxides.

6. Conclusions and Prospects

In this review, smart designs of Ni-based catalysts are discussed in four categories, including surface regulation, oxygen defects and interfacial engineering and structural optimization. In surface regulation, enhanced basicity can promote the CO_2 adsorption, resulting in active oxygen atoms which reacts with carbon species to form CO. Various oxides like La_2O_3, MgO, Ga_2O_3, and B_2O_3 can tune the surface basicity but too strong a basicity may inhibit carbon deposition. In oxygen defects, lattice distortion in perovskite structures, redox property of rare earth and lattice oxygen of transition metal oxides can promote the oxygen mobility, thus facilitating the oxidation of CH_x and C deposits to form CO and H_2. In interfacial engineering, doping noble metals can enhance the reducibility of Ni, prevent Ni from agglomeration and impede the metal oxidation. Transition metals with oxygen affinity or redox cycle can absorb more CO_2 to produce CO and oxygen atoms, accelerating the carbon removal. Besides the Ni-metal synergy, a strong MSI can slow the reduction and retard the migration of Ni, thus leading to a high dispersion on the support, such as MgO and SiO_2. Moreover, electron perturbations of Ni from CeO_2 generate active Ni sites to adsorb and dissociate CH_4. On the other hand, the Ce^{3+} promotes the C-O bond activation in CO_2 molecules to produce oxygen atoms, leading to an improved reactivity and stability in DRM reaction. In structural optimization, porous supports and core-shell structures can enhance the surface area and provide steric hindrance, leading to a highly dispersed Ni particle and more exposure to the reactants. In this case, the activation of reactants is facilitated, and metal sintering is inhibited. Despite the progress in designing Ni-based catalysts to resist coke and sintering, there is still room for further enhancement of the catalytic performance and a clear explanation of the mechanism.

First, a facile, economical, and green preparation strategy will be beneficial to the large-scale operations of DRM reaction in industry. Multi-step reaction processes may limit the yields of the catalyst materials. Also, the cost of the raw materials should be carefully controlled to an acceptable level. Furthermore, production and dispose of waste streams are another issue to be considered.

Second, novel techniques such as plasma, light and electricity assisted catalytic process can be a promising way to avoid the high temperature activation and metal sintering. Energy efficiency and stability may be enhanced in this way.

Third, combining with membrane, CO_2 can be separated from the raw feed and simultaneously converted into valuable syngas by reforming of methane. The recent advancement of highly CO_2-permeable membranes paves the way for developing an integrated system for both CO_2 capture and conversions [192–194].

Fourth, single-site or single-atom catalysts have drawn great interest in recent years due to the high efficiency of expensive catalysts and enhanced reactivity and selectivity in various reactions. For DRM reaction, single Ni atom catalysts have been proved to be highly active. However, how to prevent the agglomeration is still waiting to be resolved.

Fifth, by using CeO_2 as the support, low temperature or even room temperature activation of the DRM reactions have been reported. This strategy can save the energy input and alleviate the metal sintering. Considering the low equilibrium conversion at these conditions, an integrated system is to be developed for an efficient and immediate recovery of the unreacted molecules to realize the chemical looping process.

Author Contributions: X.G.: Conceptualization, Data curation, Investigation, Writing—original draft, Writing—review & editing. J.A.: Writing—review & editing, Project administration, Supervision, Validation. S.K.: Funding acquisition, Resources, Project administration, Supervision, Validation. All authors have read and agreed to the published version of the manuscript.

Funding: This research was funded by Ministry of Education in Singapore (MOE) Tier 2 grant (MOE2017-T2-2-130), Singapore Agency for Science, Technology and Research (A*STAR) AME IRG grant (No. A1783c0016), National Environment Agency (NEA) in Singapore (WTE-CRP 1501-103) and Youth Innovation Talents Project of Guangdong Universities (natural science) in China (2019KQNCX098).

Conflicts of Interest: The authors declare no conflict of interest.

References

1. Das, S.; Ashok, J.; Xi, S.; Borgna, A.; Hidajat, K.; Kawi, S. Highly Dispersed Ni/Silica by Carbonization–Calcination of a Chelated Precursor for Coke-Free Dry Reforming of Methane. *ACS Appl. Energy Mater.* **2020**, *3*, 7719–7735. [CrossRef]
2. Mo, L.; Leong, K.K.M.; Kawi, S. A highly dispersed and anti-coking Ni–La_2O_3/SiO_2 catalyst for syngas production from dry carbon dioxide reforming of methane. *Catal. Sci. Technol.* **2014**, *4*, 2107–2114. [CrossRef]
3. Ashok, J.; Bian, Z.; Wang, Z.; Kawi, S. Ni-phyllosilicate structure derived Ni–SiO_2–MgO catalysts for bi-reforming applications: Acidity, basicity and thermal stability. *Catal. Sci. Technol.* **2018**, *8*, 1730–1742. [CrossRef]
4. Oemar, U.; Hidajat, K.; Kawi, S. High catalytic stability of Pd-Ni/Y_2O_3 formed by interfacial Cl for oxy-CO_2 reforming of CH_4. *Catal. Today* **2017**, *281*, 276–294. [CrossRef]
5. Dewangan, N.; Hui, W.M.; Jayaprakash, S.; Bawah, A.-R.; Poerjoto, A.J.; Jie, T.; Ashok, J.; Hidajat, K.; Kawi, S. Recent progress on layered double hydroxide (LDH) derived metal-based catalysts for CO_2 conversion to valuable chemicals. *Catal. Today* **2020**, *356*, 490–513. [CrossRef]
6. Oemar, U.; Hidajat, K.; Kawi, S. Pd–Ni catalyst over spherical nanostructured Y_2O_3 support for oxy-CO_2 reforming of methane: Role of surface oxygen mobility. *Int. J. Hydrogen Energy* **2015**, *40*, 12227–12238. [CrossRef]
7. Bian, Z.; Wang, Z.; Jiang, B.; Hongmanorom, P.; Zhong, W.; Kawi, S. A review on perovskite catalysts for reforming of methane to hydrogen production. *Renew. Sustain. Energy Rev.* **2020**, *134*, 110291. [CrossRef]
8. Li, Z.; Lin, Q.; Li, M.; Cao, J.; Liu, F.; Pan, H.; Wang, Z.; Kawi, S. Recent advances in process and catalyst for CO_2 reforming of methane. *Renew. Sustain. Energy Rev.* **2020**, *134*, 110312. [CrossRef]
9. Das, S.; Pérez-Ramírez, J.; Gong, J.; Dewangan, N.; Hidajat, K.; Gates, B.C.; Kawi, S. Core–shell structured catalysts for thermocatalytic, photocatalytic, and electrocatalytic conversion of CO_2. *Chem. Soc. Rev.* **2020**, *49*, 2937–3004. [CrossRef] [PubMed]
10. Hongmanorom, P.; Ashok, J.; Zhang, G.; Bian, Z.; Wai, M.H.; Zeng, Y.; Xi, S.; Borgna, A.; Kawi, S. Enhanced performance and selectivity of CO_2 methanation over phyllosilicate structure derived Ni-Mg/SBA-15 catalysts. *Appl. Catal. B* **2021**, *282*, 119564. [CrossRef]
11. Wai, M.H.; Ashok, J.; Dewangan, N.; Das, S.; Xi, S.; Borgna, A.; Kawi, S. Design of Ceria Catalysts for Low-Temperature CO Oxidation. *ChemCatChem* **2020**, *12*, 1–11.
12. Ashok, J.; Ang, M.L.; Kawi, S. Enhanced activity of CO_2 methanation over Ni/CeO_2-ZrO_2 catalysts: Influence of preparation methods. *Catal. Today* **2017**, *281*, 304–311. [CrossRef]
13. Ashok, J.; Pati, S.; Hongmanorom, P.; Zhang, T.; Chen, J.; Kawi, S. A review of recent catalyst advances in CO_2 methanation processes. *Catal. Today* **2020**, *356*, 471–489. [CrossRef]
14. Bian, Z.; Chan, Y.M.; Yu, Y.; Kawi, S. Morphology dependence of catalytic properties of Ni/CeO_2 for CO_2 methanation: A kinetic and mechanism study. *Catal. Today* **2020**, *347*, 31–38. [CrossRef]
15. Yu, Y.; Chan, Y.M.; Bian, Z.; Song, F.; Wang, J.; Zhong, Q.; Kawi, S. Enhanced performance and selectivity of CO_2 methanation over g-C_3N_4 assisted synthesis of Ni-CeO_2 catalyst: Kinetics and DRIFTS studies. *Int. J. Hydrogen Energy* **2018**, *43*, 15191–15204. [CrossRef]
16. Yu, Y.; Bian, Z.; Song, F.; Wang, J.; Zhong, Q.; Kawi, S. Influence of Calcination Temperature on Activity and Selectivity of Ni–CeO_2 and Ni–$Ce_{0.8}Zr_{0.2}O_2$ Catalysts for CO_2 Methanation. *Top. Catal.* **2018**, *61*, 1514–1527. [CrossRef]
17. Wang, Z.; Chen, T.; Dewangan, N.; Li, Z.; Das, S.; Pati, S.; Li, Z.; Lin, J.Y.S.; Kawi, S. Catalytic mixed conducting ceramic membrane reactors for methane conversion. *React. Chem. Eng.* **2020**, *5*, 1868–1891. [CrossRef]
18. Wang, Z.; Ashok, J.; Pu, Z.; Kawi, S. Low temperature partial oxidation of methane via $BaBi_{0.05}Co_{0.8}Nb_{0.15}O_{3-\delta}$-Ni phyllosilicate catalytic hollow fiber membrane reactor. *Chem. Eng. J.* **2017**, *315*, 315–323. [CrossRef]
19. Chen, T.; Wang, Z.; Liu, L.; Pati, S.; Wai, M.H.; Kawi, S. Coupling CO_2 separation with catalytic reverse water-gas shift reaction via ceramic-carbonate dual-phase membrane reactor. *Chem. Eng. J.* **2020**, *379*, 122182. [CrossRef]
20. Kathiraser, Y.; Wang, Z.; Kawi, S. Oxidative CO_2 Reforming of Methane in $La_{0.6}Sr_{0.4}Co_{0.8}Ga_{0.2}O_{3-\delta}$ (LSCG) Hollow Fiber Membrane Reactor. *Environ. Sci. Technol.* **2013**, *47*, 14510–14517. [CrossRef]

21. Subhasis, P.; Jangam, A.; Nikita, D.; Chen, T.; Kawi, S. Ultra-thin (~1 μm) Pd–Cu membrane reactor for coupling CO_2 hydrogenation and propane dehydrogenation applications. *J. Membr. Sci.* **2020**, *595*, 117496.
22. Hu, J.; Poelman, H.; Marin, G.B.; Detavernier, C.; Kawi, S.; Galvita, V.V. FeO controls the sintering of iron-based oxygen carriers in chemical looping CO_2 conversion. *J. CO_2 Util.* **2020**, *40*, 101216. [CrossRef]
23. Liu, L.; Das, S.; Chen, T.; Dewangan, N.; Ashok, J.; Xi, S.; Borgna, A.; Li, Z.; Kawi, S. Low temperature catalytic reverse water-gas shift reaction over perovskite catalysts in DBD plasma. *Appl. Catal. B* **2020**, *265*, 118573. [CrossRef]
24. Liu, L.; Zhang, Z.; Das, S.; Xi, S.; Kawi, S. $LaNiO_3$ as a precursor of Ni/La_2O_3 for reverse water-gas shift in DBD plasma: Effect of calcination temperature. *Energy Convers. Manag.* **2020**, *206*, 112475. [CrossRef]
25. Maneerung, T.; Hidajat, K.; Kawi, S. Co-production of hydrogen and carbon nanofibers from catalytic decomposition of methane over $LaNi_{(1-x)}M_xO_{3-\alpha}$ perovskite (where M = Co, Fe and X = 0, 0.2, 0.5, 0.8, 1). *Int. J. Hydrogen Energy* **2015**, *40*, 13399–13411. [CrossRef]
26. Bian, Z.F.; Das, S.; Wai, M.H.; Hongmanorom, P.; Kawi, S. A Review on Bimetallic Nickel-Based Catalysts for CO_2 Reforming of Methane. *ChemPhysChem* **2017**, *18*, 3117–3134. [CrossRef]
27. Li, Z.W.; Li, M.; Bian, Z.F.; Kathiraser, Y.; Kawi, S. Design of highly stable and selective core/yolk–shell nanocatalysts-A review. *Appl. Catal. B* **2016**, *188*, 324–341. [CrossRef]
28. Kathiraser, Y.; Oemar, U.; Saw, E.T.; Li, Z.W.; Kawi, S. Kinetic and mechanistic aspects for CO_2 reforming of methane over Ni based catalysts. *Chem. Eng. J.* **2015**, *278*, 62–78. [CrossRef]
29. Bian, Z.F.; Kawi, S. Preparation, characterization and catalytic application of phyllosilicate: A review. *Catal. Today* **2020**, *339*, 3–23. [CrossRef]
30. Kawi, S.; Kathiraser, Y.; Ni, J.; Oemar, U.; Li, Z.W.; Saw, E.T. Progress in Synthesis of Highly Active and Stable Nickel-Based Catalysts for Carbon Dioxide Reforming of Methane. *ChemSusChem* **2015**, *8*, 3556–3575. [CrossRef]
31. Li, Z.W.; Das, S.; Hongmanorom, P.; Dewangan, N.; Wai, M.H.; Kawi, S. Silica-based micro- and mesoporous catalysts for dry reforming of methane. *Catal. Sci. Technol.* **2018**, *8*, 2763–2778. [CrossRef]
32. Bradford, M.C.J.; Vannice, M.A. Catalytic reforming of methane with carbon dioxide over nickel catalysts I. Catalyst characterization and activity. *Appl. Catal. A* **1996**, *142*, 73–96. [CrossRef]
33. Gadalla, A.M.; Bower, B. The role of catalyst support on the activity of nickel for reforming methane with CO_2. *Chem. Eng. Sci.* **1988**, *43*, 3049–3062. [CrossRef]
34. Chubb, T.A. Characteristics of CO_2/CH_4 reforming-methanation cycle relevant to the solchem thermochemical power system. *Sol. Energy* **1980**, *24*, 342–345. [CrossRef]
35. McCrary, J.H.; McCrary, G.E.; Chubb, T.A.; Nemecek, J.J.; Simmons, D.E. An experimental study of the CO_2-CH_4 reforming-methanation cycle as a mechanism for converting and transporting solar energy. *Sol. Energy* **1982**, *29*, 141–151. [CrossRef]
36. Kaichev, V.V.; Gladky, A.Y.; Prosvirin, I.P.; Saraev, A.A.; Hävecker, M.; Knop-Gericke, A.; Schlögl, R.; Bukhtiyarov, V.I. In situ XPS study of self-sustained oscillations in catalytic oxidation of propane over nickel. *Surf. Sci.* **2013**, *609*, 113–118. [CrossRef]
37. Ni, J.; Zhao, J.; Chen, L.W.; Lin, J.Y.; Kawi, S. Lewis Acid Sites Stabilized Nickel Catalysts for Dry (CO_2) Reforming of Methane. *ChemCatChem* **2016**, *8*, 3732–3739. [CrossRef]
38. Wang, C.; Sun, N.; Kang, M.; Wen, X.; Zhao, N.; Xiao, F.; Wei, W.; Zhao, T.; Sun, Y. The bi-functional mechanism of CH4 dry reforming over a Ni–CaO–ZrO_2 catalyst: Further evidence via the identification of the active sites and kinetic studies. *Catal. Sci. Technol.* **2013**, *3*, 2435–2443. [CrossRef]
39. Al-Fatesh, A.S.; Arafat, Y.; Atia, H.; Ibrahim, A.A.; Ha, Q.L.M.; Schneider, M.; M-Pohl, M.; Fakeeha, A.H. CO_2-reforming of methane to produce syngas over Co-Ni/SBA-15 catalyst: Effect of support modifiers (Mg, La and Sc) on catalytic stability. *J. CO_2 Util.* **2017**, *21*, 395–404. [CrossRef]
40. Phan, T.S.; Sane, A.R.; de Vasconcelos, B.R.; Nzihou, A.; Sharrock, P.; Grouset, D.; Minh, D.P. Hydroxyapatite supported bimetallic cobalt and nickel catalysts for syngas production from dry reforming of methane. *Appl. Catal. B* **2018**, *224*, 310–321. [CrossRef]
41. Zhang, L.; Lian, J.; Li, L.; Peng, C.; Liu, W.M.; Xu, X.L.; Fang, X.Z.; Wang, Z.; Wang, X.; Peng, H.E. $LaNiO_3$ nanocube embedded in mesoporous silica for dry reforming of methane with enhanced coking resistance. *Microporous Mesoporous Mater.* **2018**, *266*, 189–197. [CrossRef]
42. Li, X.Y.; Li, D.; Tian, H.; Zeng, L.; Zhao, J.-Z.; Gong, J.L. Dry reforming of methane over Ni/La_2O_3 nanorod catalysts with stabilized Ni nanoparticles. *Appl. Catal. B* **2017**, *202*, 683–694. [CrossRef]

43. Zhang, Z.; Verykios, X.E.; MacDonald, S.; Affrossman, S. Comparative Study of Carbon Dioxide Reforming of Methane to Synthesis Gas over Ni/La_2O_3 and Conventional Nickel-Based Catalysts. *J. Phys. Chem.* **1996**, *100*, 744–752. [CrossRef]
44. Jabbour, K.; Massiani, P.; Davidson, A.; Casale, S.; El Hassan, N. Ordered mesoporous "one-pot" synthesized Ni-Mg(Ca)-Al_2O_3 as effective and remarkably stable catalysts for combined steam and dry reforming of methane (CSDRM). *Appl. Catal. B* **2017**, *201*, 527–542. [CrossRef]
45. Fang, X.Z.; Zhang, J.; Liu, J.J.; Wang, C.; Huang, Q.; Xu, X.L.; Peng, H.G.; Liu, W.M.; Wang, X.; Zhou, W.F. Methane dry reforming over Ni/Mg-Al-O: On the significant promotional effects of rare earth Ce and Nd metal oxides. *J. CO_2 Util.* **2018**, *25*, 242–253. [CrossRef]
46. Zuo, Z.J.; Liu, S.Z.; Wang, Z.C.; Liu, C.; Huang, W.; Huang, J.; Liu, P. Dry Reforming of Methane on Single-Site Ni/MgO Catalysts: Importance of Site Confinement. *ACS Catal.* **2018**, *8*, 9821–9835. [CrossRef]
47. Feng, X.Q.; Liu, J.; Zhang, P.; Zhang, Q.; Xu, L.Y.; Zhao, L.P.; Song, X.F.; Gao, L. Highly coke resistant Mg–Ni/Al_2O_3 catalyst prepared via a novel magnesiothermic reduction for methane reforming catalysis with CO_2: The unique role of Al–Ni intermetallics. *Nanoscale* **2019**, *11*, 1262–1272. [CrossRef]
48. Ni, J.; Chen, L.W.; Lin, J.Y.; Schreyer, M.K.; Wang, Z.; Kawi, S. High performance of Mg–La mixed oxides supported Ni catalysts for dry reforming of methane: The effect of crystal structure. *Int. J. Hydrogen Energy* **2013**, *38*, 13631–13642. [CrossRef]
49. Li, K.; He, F.; Yu, H.M.; Wang, Y.; Wu, Z.J. Theoretical study on the reaction mechanism of carbon dioxide reforming of methane on La and La_2O_3 modified Ni(111) surface. *J. Catal.* **2018**, *364*, 248–261. [CrossRef]
50. Dębek, R.; Motak, M.; Galvez, M.E.; Da Costa, P.; Grzybek, T. Catalytic activity of hydrotalcite-derived catalysts in the dry reforming of methane: On the effect of Ce promotion and feed gas composition. *Reac. Kinet. Mech. Cat.* **2017**, *121*, 185–208. [CrossRef]
51. Pan, X.Y.; Kuai, P.; Liu, Y.; Ge, Q.; Liu, C.J. Promotion effects of Ga_2O_3 on CO_2 adsorption and conversion over a SiO_2-supported Nicatalyst. *Energy Environ. Sci.* **2010**, *3*, 1322–1325. [CrossRef]
52. Ni, J.; Chen, L.; Lin, J.; Kawi, S. Carbon deposition on borated alumina supported nano-sized Ni catalysts for dry reforming of CH_4. *Nano Energy* **2012**, *1*, 674–686. [CrossRef]
53. Dębek, R.; Motak, M.; Galvez, M.E.; Grzybek, T.; Da Costa, P. Influence of Ce/Zr molar ratio on catalytic performance of hydrotalcite-derived catalysts at low temperature CO_2 methane reforming. *Int. J. Hydrogen Energy* **2017**, *42*, 23556–23567. [CrossRef]
54. Świrk, K.; Gálvez, M.E.; Motak, M.; Grzybek, T.; Rønning, M.; Da Costa, P. Yttrium promoted Ni-based double-layered hydroxides for dry methane reforming. *J. CO_2 Util.* **2018**, *27*, 247–258. [CrossRef]
55. Świrk, K.; Zhang, H.; Li, S.; Chen, Y.; Rønning, M.; Motak, M.; Grzybek, T.; Da Costa, P. Carbon-resistant NiO-Y_2O_3-nanostructured catalysts derived from double-layered hydroxides for dry reforming of methane. *Catal. Today* **2020**, in press.
56. Liu, H.; Wierzbicki, D.; Debek, R.; Motak, M.; Grzybek, T.; Da Costa, P.; Gálvez, M.E. La-promoted Ni-hydrotalcite-derived catalysts for dry reforming of methane at low temperatures. *Fuel* **2016**, *182*, 8–16. [CrossRef]
57. Sun, G.B.; Hidajat, K.; Wu, X.S.; Kawi, S. A crucial role of surface oxygen mobility on nanocrystalline Y_2O_3 support for oxidative steam reforming of ethanol to hydrogen over Ni/Y_2O_3 catalysts. *Appl. Catal. B* **2008**, *81*, 303–312. [CrossRef]
58. Lian, Z.; Olanrele, S.O.; Si, C.W.; Yang, M.; Li, B. Critical Role of Interfacial Sites between Nickel and CeO_2 Support in Dry Reforming of Methane: Revisit of Reaction Mechanism and Origin of Stability. *J. Phys. Chem. C* **2020**, *124*, 5118–5124. [CrossRef]
59. Sun, N.; Wen, X.; Wang, F.; Peng, W.; Zhao, N.; Xiao, F.K.; Wei, W.; Sun, Y.H.; Kang, J.T. Catalytic performance and characterization of Ni–CaO–ZrO_2 catalysts for dry reforming of methane. *Appl. Surf. Sci.* **2011**, *257*, 9169–9176. [CrossRef]
60. Tao, Q.Q.; Wang, Z.D.; Bandara, J.; Guo, C.Q.; Gan, Y.; Zhang, L.; Lu, Z.X.; Tan, H.Y.; Yan, C.F. Enhanced catalytic activity of Ni–Mo_2C/La_2O_3–ZrO_2 bifunctional catalyst for dry reforming of methane. *J. Mater. Sci.* **2018**, *53*, 14559–14572. [CrossRef]
61. Jang, W.J.; Shim, J.O.; Kim, H.M.; Yoo, S.Y.; Roh, H.S. A review on dry reforming of methane in aspect of catalytic properties. *Catal. Today* **2019**, *324*, 15–26. [CrossRef]

62. Wang, F.; Xu, L.; Yang, J.; Zhang, J.; Zhang, L.; Li, H.; Zhao, Y.; Li, H.X.; Wu, K.; Xu, G.Q.; et al. Enhanced catalytic performance of Ir catalysts supported on ceria-based solid solutions for methane dry reforming reaction. *Catal. Today* **2017**, *281*, 295–303. [CrossRef]
63. Ay, H.; Üner, D. Dry reforming of methane over CeO_2 supported Ni, Co and Ni–Co catalysts. *Appl. Catal. B* **2015**, *179*, 128–138. [CrossRef]
64. Elsayed, N.H.; Roberts, N.R.M.; Joseph, B.; Kuhn, J.N. Low temperature dry reforming of methane over Pt–Ni–Mg/ceria–zirconia catalysts. *Appl. Catal. B* **2015**, *179*, 213–219. [CrossRef]
65. Liu, Z.Y.; Grinter, D.C.; Lustemberg, P.G.; Nguyen-Phan, T.-D.; Zhou, Y.H.; Luo, S.; Waluyo, I.; Crumlin, E.J.; Stacchiola, D.J.; Zhou, J.; et al. Dry Reforming of Methane on a Highly-Active Ni-CeO_2 Catalyst: Effects of Metal-Support Interactions on C−H Bond Breaking. *Angew. Chem. Int. Ed.* **2016**, *55*, 7455–7459. [CrossRef] [PubMed]
66. Vasiliades, M.A.; Makri, M.M.; Djinović, P.; Erjavec, B.; Pintar, A.; Efstathiou, A.M. Dry reforming of methane over 5 wt% Ni/$Ce_{1-x}Pr_xO_{2-\delta}$ catalysts: Performance and characterisation of active and inactive carbon by transient isotopic techniques. *Appl. Catal. B* **2016**, *197*, 168–183. [CrossRef]
67. Lustemberg, P.G.; Ramírez, P.J.; Liu, Z.Y.; Gutiérrez, R.A.; Grinter, D.G.; Carrasco, J.; Senanayake, S.D.; Rodriguez, J.A.; Ganduglia-Pirovano, M.V. Room-Temperature Activation of Methane and Dry Re-forming with CO_2 on Ni-CeO_2(111) Surfaces: Effect of Ce^{3+} Sites and Metal–Support Interactions on C–H Bond Cleavage. *ACS Catal.* **2016**, *6*, 8184–8191. [CrossRef]
68. Löfberg, A.; Guerrero-Caballero, J.; Kane, T.; Rubbens, A.; Jalowiecki-Duhamel, L. Ni/CeO_2 based catalysts as oxygen vectors for the chemical looping dry reforming of methane for syngas production. *Appl. Catal. B* **2017**, *212*, 159–174. [CrossRef]
69. Akri, M.; Pronier, S.; Chafik, T.; Achak, O.; Granger, P.; Simon, P.; Trentesaux, M.; Batiot-Dupeyrat, C. Development of nickel supported La and Ce-natural illite clay for autothermal dry reforming of methane: Toward a better resistance to deactivation. *Appl. Catal. B* **2017**, *205*, 519–531. [CrossRef]
70. Gurav, H.R.; Dama, S.; Samuel, V.; Chilukuri, S. Influence of preparation method on activity and stability of Ni catalysts supported on Gd doped ceria in dry reforming of methane. *J. CO_2 Util.* **2017**, *20*, 357–367. [CrossRef]
71. Shamskar, F.R.; Meshkani, F.; Rezaei, M. Preparation and characterization of ultrasound-assisted co-precipitated nanocrystalline La-, Ce-, Zr –promoted Ni-Al_2O_3 catalysts for dry reforming reaction. *J. CO_2 Util.* **2017**, *22*, 124–134. [CrossRef]
72. Le Saché, E.; Santos, J.L.; Smith, T.J.; Centeno, M.A.; Arellano-Garcia, H.; Odriozola, J.A.; Reina, T.R. Multicomponent Ni-CeO_2 nanocatalysts for syngas production from CO_2/CH_4 mixtures. *J. CO_2 Util.* **2018**, *25*, 68–78. [CrossRef]
73. Damyanova, S.; Pawelec, B.; Palcheva, R.; Karakirova, Y.; Sanchez, M.C.C.; Tyuliev, G.; Gaigneaux, E.; Fierro, J.L.G. Structure and surface properties of ceria-modified Ni-based catalysts for hydrogen production. *Appl. Catal. B* **2018**, *225*, 340–353. [CrossRef]
74. Liu, Y.; Wu, Y.; Akhtamberdinova, Z.; Chen, X.P.; Jiang, G.D.; Liu, D. Dry Reforming of Shale Gas and Carbon Dioxide with Ni-Ce-Al_2O_3 Catalyst: Syngas Production Enhanced over Ni-CeO_x Formation. *ChemCatChem* **2018**, *10*, 4689–4698. [CrossRef]
75. Luisetto, I.; Tuti, S.; Romano, C.; Boaro, M.; Di Bartolomeo, E.; Kesavan, J.K.; Kumar, S.M.S.; Selvakumar, K. Dry reforming of methane over Ni supported on doped CeO_2: New insight on the role of dopants for CO_2 activation. *J. CO_2 Util.* **2019**, *30*, 63–78. [CrossRef]
76. Yan, X.L.; Hu, T.; Liu, P.; Li, S.; Zhao, B.; Zhang, Q.; Jiao, W.Y.; Chen, S.; Wang, P.F.; Lu, J.J.; et al. Highly efficient and stable Ni/CeO_2-SiO_2 catalyst for dry reforming of methane: Effect of interfacial structure of Ni/CeO_2 on SiO_2. *Appl. Catal. B* **2019**, *246*, 221–231. [CrossRef]
77. Sagar, T.V.; Padmakar, D.; Lingaiah, N.; Prasad, P.S.S. Influence of Solid Solution Formation on the Activity of CeO_2 Supported Ni–Cu Mixed Oxide Catalysts in Dry Reforming of Methane. *Catal. Lett.* **2019**, *149*, 2597–2606. [CrossRef]
78. Abdulrasheed, A.; Jalil, A.A.; Gambo, Y.; Ibrahim, M.; Hambali, H.U.; Hamid, M.Y.S. A review on catalyst development for dry reforming of methane to syngas: Recent advances. *Renew. Sustain. Energy Rev.* **2019**, *108*, 175–193. [CrossRef]
79. Macario, A.; Frontera, P.; Candamano, S.; Crea, F.; De Luca, P.; Antonucci, P.L. Nanostructured Catalysts for Dry-Reforming of Methane. *J. Nanosci. Nanotechnol.* **2019**, *19*, 3135–3147. [CrossRef]

80. Laosiripojana, N.; Assabumrungrat, S. Catalytic dry reforming of methane over high surface area ceria. *Appl. Catal. B* **2005**, *60*, 107–116. [CrossRef]
81. Horváth, A.; Stefler, G.; Geszti, O.; Kienneman, A.; Pietraszek, A.; Guczi, L. Methane dry reforming with CO_2 on CeZr-oxide supported Ni, NiRh and NiCo catalysts prepared by sol–gel technique: Relationship between activity and coke formation. *Catal. Today* **2011**, *169*, 102–111. [CrossRef]
82. Safavinia, B.; Wang, Y.M.; Jiang, C.Y.; Roman, C.; Darapaneni, P.; Larriviere, J.; Cullen, D.A.; Dooley, K.M.; Dorman, J.A. Enhancing $Ce_xZr_{1-x}O_2$ Activity for Methane Dry Reforming Using Subsurface Ni Dopants, Role of catalyst support over PdO–NiO catalysts on catalyst activity and stability for oxy-CO_2 reforming of methane. *ACS Catal.* **2020**, *10*, 4070–4079. [CrossRef]
83. Oemar, U.; Hidajat, K.; Kawi, S. Role of catalyst support over PdO–NiO catalysts on catalyst activity and stability for oxy-CO_2 reforming of methane. *Appl. Catal. A* **2011**, *402*, 176–187. [CrossRef]
84. Sutthiumporn, K.; Kawi, S. Promotional effect of alkaline earth over Ni–La_2O_3 catalyst for CO_2 reforming of CH_4: Role of surface oxygen species on H_2 production and carbon suppression. *Int. J. Hydrogen Energy* **2011**, *36*, 14435–14446. [CrossRef]
85. Pino, L.; Italiano, C.; Vita, A.; Laganà, M.; Recupero, V. $Ce_{0.70}La_{0.20}Ni_{0.10}O_{2-\delta}$ catalyst for methane dry reforming: Influence of reduction temperature on the catalytic activity and stability. *Appl. Catal. B* **2017**, *218*, 779–792. [CrossRef]
86. Yang, W.Q.; Wang, Z.B.; Tan, W.Z.; Peng, R.R.; Wu, X.J.; Lu, Y.L. First principles study on methane reforming over Ni/TiO_2(110) surface in solid oxide fuel cells under dry and wet atmospheres. *Sci. China Mater.* **2020**, *63*, 364–374. [CrossRef]
87. Lou, Y.; Steib, M.; Zhang, Q.; Tiefenbacher, K.; Horváth, A.; Jentys, A.; Liu, Y.; Lercher, J.A. Design of stable Ni/ZrO_2 catalysts for dry reforming of methane. *J. Catal.* **2017**, *356*, 147–156. [CrossRef]
88. Wang, Y.; Yao, L.; Wang, Y.; Wang, S.H.; Zhao, Q.; Mao, D.H.; Hu, C.W. Low-Temperature Catalytic CO_2 Dry Reforming of Methane on Ni-Si/ZrO_2 Catalyst. *ACS Catal.* **2018**, *8*, 6495–6506. [CrossRef]
89. Liu, W.M.; Li, L.; Zhang, X.H.; Wang, Z.; Wang, X.; Peng, H.G. Design of Ni-ZrO_2@SiO_2 catalyst with ultra-high sintering and coking resistance for dry reforming of methane to prepare syngas. *J. CO_2 Util.* **2018**, *27*, 297–307. [CrossRef]
90. Zhang, M.; Zhang, J.F.; Wu, Y.Q.; Pan, J.X.; Zhang, Q.D.; Tan, Y.S.; Han, Y.Z. Insight into the effects of the oxygen species over Ni/ZrO_2 catalyst surface on methane reforming with carbon dioxide. *Appl. Catal. B* **2019**, *244*, 427–437. [CrossRef]
91. Peña, M.A.; Fierro, J.L.G. Chemical Structures and Performance of Perovskite Oxides. *Chem. Rev.* **2001**, *101*, 1981–2018. [CrossRef] [PubMed]
92. Royer, S.; Duprez, D. Catalytic Oxidation of Carbon Monoxide over Transition Metal Oxides. *ChemCatChem* **2011**, *3*, 24–65. [CrossRef]
93. Kim, C.H.; Qi, G.; Dahlbery, K.; Li, W. Strontium-Doped Perovskites Rival Platinum Catalysts for Treating NO_x in Simulated Diesel Exhaust. *Science* **2010**, *327*, 1624–1627. [CrossRef] [PubMed]
94. Gomez-Cuaspud, J.; Perez, C.A.; Schmal, M. Nanostructured $La_{0.8}Sr_{0.2}Fe_{0.8}Cr_{0.2}O_3$ Perovskite for the Steam Methane Reforming. *Catal. Lett.* **2016**, *146*, 2504–2515. [CrossRef]
95. Gomez-Cuaspud, J.A.; Vera-Lopez, E.; Carda-Castello, J.B.; Barrachina-Albert, E. One-step hydrothermal synthesis of $LaFeO_3$ perovskite for methane steam reforming. *React. Kinet. Mech. Catal.* **2016**, *120*, 167–179. [CrossRef]
96. Di Bartolomeo, E.; Basoli, F.; Luisetto, I.; Tuti, S.; Zurlo, F.; Salehi, Z.; Licoccia, S. Ni and Ni-Co $La_{0.8}Sr_{0.2}Ga_{0.8}Mg_{0.2}O_{3-\delta}$ infiltrated cells in H_2 and CH_4/CO_2 mixture. *Appl. Catal. B* **2016**, *191*, 1–7. [CrossRef]
97. Messaoudi, H.; Thomas, S.; Djaidja, A.; Slyemi, S.; Barama, A. Study of La_xNiO_y and $La_xNiO_y/MgAl_2O_4$ catalysts in dry reforming of methane. *J. CO_2 Util.* **2018**, *24*, 40–49. [CrossRef]
98. Kang, D.; Lim, H.S.; Lee, M.; Lee, J.W. Syngas production on a Ni-enhanced Fe_2O_3/Al_2O_3 oxygen carrier via chemical looping partial oxidation with dry reforming of methane. *Appl. Energy* **2018**, *211*, 174–186. [CrossRef]
99. Fan, M.S.; Abdullah, A.Z.; Bhatia, S. Catalytic Technology for Carbon Dioxide Reforming of Methane to Synthesis Gas. *ChemCatChem* **2009**, *1*, 192–208. [CrossRef]

100. Pakhare, D.; Schwartz, V.; Abdelsayed, V.; Haynes, D.; Shekhawat, D.; Puston, J.; Spivey, J. Kinetic and mechanistic study of dry (CO_2) reforming of methane over Rh-substituted $La_2Zr_2O_7$ pyrochlores. *J. Catal.* **2014**, *316*, 78–92. [CrossRef]
101. Wang, H.Q.; Dong, X.L.; Zhao, T.T.; Yu, H.R.; Li, M. Dry reforming of methane over bimetallic Ni-Co catalyst prepared from $La(Co_xNi_{1-x})_{0.5}Fe_{0.5}O_3$ perovskite precursor: Catalytic activity and coking resistance. *Appl. Catal. B* **2019**, *245*, 302–313. [CrossRef]
102. Yang, E.H.; Noh, Y.S.; Hong, G.H.; Moon, D.J. Combined steam and CO_2 reforming of methane over $La_{1-x}Sr_xNiO_3$ perovskite oxides. *Catal. Today.* **2018**, *299*, 242–250. [CrossRef]
103. Rynkowski, J.; Samulkiewicz, P.; Ladavos, A.; Pomonis, P. Catalytic performance of reduced $La_{2-x}Sr_xNiO_4$ perovskite-like oxides for CO_2 reforming of CH_4. *Appl. Catal. A* **2004**, *263*, 1–9. [CrossRef]
104. Sutthiumporn, K.; Maneerung, T.; Kathiraser, Y.; Kawi, S. CO_2 dry-reforming of methane over $La_{0.8}Sr_{0.2}Ni_{0.8}M_{0.2}O_3$ perovskite (M = Bi, Co, Cr, Cu, Fe): Roles of lattice oxygen on C–H activation and carbon suppression. *Int. J. Hydrogen Energy* **2012**, *37*, 11195–11207. [CrossRef]
105. Tsoukalou, A.; Imtiaz, Q.; Kim, S.M.; Abdala, P.M.; Yoon, S.; Müller, C.R. Dry-reforming of methane over bimetallic Ni–M/La_2O_3 (M = Co, Fe): The effect of the rate of $La_2O_2CO_3$ formation and phase stability on the catalytic activity and stability. *J. Catal.* **2016**, *343*, 208–214. [CrossRef]
106. Wang, M.; Zhao, T.T.; Dong, X.L.; Li, M.; Wang, H.Q. Effects of Ce substitution at the A-site of $LaNi_{0.5}Fe_{0.5}O_3$ perovskite on the enhanced catalytic activity for dry reforming of methane. *Appl. Catal. B* **2018**, *224*, 214–221. [CrossRef]
107. Figueredo, G.P.; Medeiros, R.L.B.A.; Macedo, H.P.; De Oliveira, Â.A.S.; Braga, R.M.; Mercury, J.M.R.; Melo, M.A.F. A comparative study of dry reforming of methane over nickel catalysts supported on perovskite-type $LaAlO_3$ and commercial α-Al_2O_3. *Int. J. Hydrogen Energy* **2018**, *43*, 11022–11037. [CrossRef]
108. Ruckenstein, E.; Hu, Y.H. Role of Support in CO_2 Reforming of CH_4 to Syngas over Ni Catalysts. *J. Catal.* **1996**, *162*, 230–238. [CrossRef]
109. Foley, H.C.; Hong, A.J.; Brinen, J.S.; Allard, L.F.; Garrat-Reed, A.J. Bimetallic catalysts comprised of dissimilar metals for the reduction of carbon monoxide with hydrogen. *Appl. Catal.* **1990**, *61*, 351–375. [CrossRef]
110. Fan, C.; Zhu, Y.A.; Xu, Y.; Zhou, Y.; Zhou, X.G.; Chen, D. Origin of synergistic effect over Ni-based bimetallic surfaces: A density functional theory study. *J. Chem. Phys.* **2012**, *137*, 014703. [CrossRef]
111. De, S.; Zhang, J.; Luque, R.; Yan, N. Ni-based bimetallic heterogeneous catalysts for energy and environmental applications. *Energy Environ. Sci.* **2016**, *9*, 3314–3347. [CrossRef]
112. Tanksale, A.; Beltramini, J.N.; Dumesic, J.A.; Lu, G.Q. Effect of Pt and Pd promoter on Ni supported catalysts—A TPR/TPO/TPD and microcalorimetry study. *J. Catal.* **2008**, *258*, 366–377. [CrossRef]
113. Zhang, H.; Dai, B.; Wang, X.; Li, W.; Han, Y.; Gu, J.; Zhang, J. Non-mercury catalytic acetylene hydrochlorination over bimetallic Au–Co(III)/SAC catalysts for vinyl chloride monomer production. *Green Chem.* **2013**, *15*, 829–836. [CrossRef]
114. Sankar, M.; Dimitratos, N.; Miedziak, P.J.; Wells, P.P.; Kiely, C.J.; Hutchings, G.J. Designing bimetallic catalysts for a green and sustainable future. *Chem. Soc. Rev.* **2012**, *41*, 8099–8139. [CrossRef] [PubMed]
115. Roy, S.; Hariharan, S.; Tiwari, A.K. Pt–Ni Subsurface Alloy Catalysts: An Improved Performance toward CH_4 Dissociation. *J. Phys. Chem. C* **2018**, *122*, 10857–10870. [CrossRef]
116. Lee, J.H.; Lee, E.G.; Joo, O.S.; Jung, K.D. Stabilization of Ni/Al_2O_3 catalyst by Cu addition for CO_2 reforming of methane. *Appl. Catal. A* **2004**, *269*, 1–6. [CrossRef]
117. Fan, M.S.; Abdullah, A.Z.; Bhatia, S. Utilization of Greenhouse Gases through Dry Reforming: Screening of Nickel-Based Bimetallic Catalysts and Kinetic Studies. *ChemSusChem* **2011**, *4*, 1643–1653. [CrossRef]
118. Kambolis, A.; Matralis, H.; Trovarelli, A.; Papadopoulou, C. Ni/CeO_2-ZrO_2 catalysts for the dry reforming of methane. *Appl. Catal. A* **2010**, *377*, 16–26. [CrossRef]
119. Li, L.; Zhou, L.; Ould-Chikh, S.; Anjum, D.H.; Kanoun, M.B.; Scaranto, J.; Hedhili, M.N.; Khalid, S.; Laveille, V.P.; D'Souza, L.; et al. Controlled Surface Segregation Leads to Efficient Coke-Resistant Nickel/Platinum Bimetallic Catalysts for the Dry Reforming of Methane. *ChemCatChem* **2015**, *7*, 819–829. [CrossRef]
120. Lucci, F.R.; Marcinkowski, M.D.; Lawton, T.J.; Sykes, E.C.H. H_2 Activation and Spillover on Catalytically Relevant Pt–Cu Single Atom Alloys. *J. Phys. Chem. C* **2015**, *119*, 24351–24357. [CrossRef]
121. Tomishige, K.; Kanazawa, S.; Ito, S.-I.; Kunimori, K. Catalyst development for direct heat supply from combustion to reforming in methane reforming with CO_2 and O_2. *Appl. Catal. A* **2003**, *244*, 71–82. [CrossRef]

122. Kim, J.; Park, W.H.; Doh, W.H.; Lee, S.W.; Noh, M.C.; Gallet, J.-J.; Bournel, F.; Kondoh, H.; Mase, K.; Jung, Y.; et al. Adsorbate-driven reactive interfacial Pt-NiO_{1-x} nanostructure formation on the $Pt_3Ni(111)$ alloy surface. *Sci. Adv.* **2018**, *4*, eaat3151. [CrossRef] [PubMed]
123. Kim, S.T.; Kim, J.; Song, H.C.; Kim, D.; Jeong, B.; Lee, J.; Shin, J.W.; Ryoo, R.; Park, J.Y. Catalytic Synergy on PtNi Bimetal Catalysts Driven by Interfacial Intermediate Structures. *ACS Catal.* **2020**, *10*, 10459–10467. [CrossRef]
124. Mukainakano, Y.; Yoshida, K.; Okumura, K.; Kunimori, K.; Tomishige, K. Catalytic performance and QXAFS analysis of Ni catalysts modified with Pd for oxidative steam reforming of methane. *Catal. Today* **2008**, *132*, 101–108. [CrossRef]
125. AlSabban, B.; Falivene, L.; Kozlov, S.M.; Aguilar-Tapia, A.; Ould-Chikh, S.; Hazemann, J.-L.; Cavallo, L.; Basset, J.-M.; Takanabe, K. In-operando elucidation of bimetallic CoNi nanoparticles during high-temperature CH_4/CO_2 reaction. *Appl. Catal. B* **2017**, *213*, 177–189. [CrossRef]
126. Margossian, T.; Larmier, K.; Kim, S.M.; Krumeich, F.; Muller, C.; Copéret, C. Supported Bimetallic NiFe Nanoparticles through Colloid Synthesis for Improved Dry Reforming Performance. *ACS Catal.* **2017**, *7*, 6942–6948. [CrossRef]
127. Bian, Z.F.; Kawi, S. Highly carbon-resistant Ni–Co/SiO_2 catalysts derived from phyllosilicates for dry reforming of methane. *J. CO_2 Util.* **2017**, *18*, 345–352. [CrossRef]
128. Das, S.; Sengupta, M.; Bag, A.; Shah, M.; Bordoloi, A. Facile synthesis of highly disperse Ni–Co nanoparticles over mesoporous silica for enhanced methane dry reforming. *Nanoscale* **2018**, *10*, 6409–6425. [CrossRef]
129. Wu, Z.X.; Yang, B.; Miao, S.; Liu, W.; Xie, J.L.; Lee, S.; Pellin, M.J.; Xiao, D.Q.; Su, D.S.; Ma, D. Lattice Strained Ni-Co alloy as a High-Performance Catalyst for Catalytic Dry Reforming of Methane. *ACS Catal.* **2019**, *9*, 2693–2700. [CrossRef]
130. Nagaoka, K.; Takanabe, K.; Aika, K.-I. Modification of Co/TiO_2 for dry reforming of methane at 2 MPa by Pt, Ru or Ni. *Appl. Catal. A* **2004**, *268*, 151–158. [CrossRef]
131. Jones, G.; Jakobsen, G.J.; Shim, S.S.; Kleis, J.; Andersson, M.P.; Rossmeisl, J.; Abild-Pedersen, F.; Bligaard, T.; Helveg, S.; Hinnemann, B.; et al. First principles calculations and experimental insight into methane steam reforming over transition metal catalysts. *J. Catal.* **2008**, *259*, 147–160. [CrossRef]
132. Fan, X.; Liu, Z.; Zhu, Y.-A.; Tong, G.; Zhang, J.; Engelbrekt, C.; Ulstrup, J.; Zhu, K.; Zhou, X. Tuning the composition of metastable $Co_xNi_yMg_{100-x-y}(OH)(OCH_3)$ nanoplates for optimizing robust methane dry reforming catalyst. *J. Catal.* **2015**, *330*, 106–119. [CrossRef]
133. Gao, X.Y.; Ashok, J.; Widjaja, S.; Hidajat, K.; Kawi, S. Ni/SiO_2 catalyst prepared via Ni-aliphatic amine complexation for dry reforming of methane: Effect of carbon chain number and amine concentration. *Appl. Catal. A* **2015**, *503*, 34–42. [CrossRef]
134. Tu, W.; Ghoussoub, M.; Singh, C.V.; Chin, C.Y.-H. Molecularly Tailored Nickel Precursor and Support Yield a Stable Methane Dry Reforming Catalyst with Superior Metal Utilization. *J. Am. Chem. Soc.* **2017**, *139*, 6928–6945. [CrossRef]
135. Theofanidis, S.A.; Galvita, V.V.; Poelman, H.; Marin, G.B. Enhanced Carbon-Resistant Dry Reforming Fe-Ni Catalyst: Role of Fe. *ACS Catal.* **2015**, *5*, 3028–3039. [CrossRef]
136. Theofanidis, S.A.; Batchu, R.; Galvita, V.V.; Poelman, H.; Marin, G.B. Carbon gasification from Fe–Ni catalysts after methane dry reforming. *Appl. Catal. B* **2016**, *185*, 42–55. [CrossRef]
137. Wu, T.; Zhang, Q.; Cai, W.; Zhang, P.; Song, X.; Sun, Z.; Gao, L. Phyllosilicate evolved hierarchical Ni- and Cu–Ni/SiO_2 nanocomposites for methane dry reforming catalysis. *Appl. Catal. A* **2015**, *503*, 94–102. [CrossRef]
138. Hou, Z.; Yokota, O.; Tanaka, T.; Yashima, T. Characterization of Ca-promoted Ni/α-Al_2O_3 catalyst for CH_4 reforming with CO_2. *Appl. Catal. A* **2003**, *253*, 381–387. [CrossRef]
139. Pakhare, D.; Spivey, J.Y. A review of dry (CO_2) reforming of methane over noble metal catalysts. *Chem. Soc. Rev.* **2014**, *43*, 7813–7837. [CrossRef]
140. Arbag, H.; Yasyerli, S.; Yasyerli, N.; Dogu, G.; Dogu, T. Enhancement of catalytic performance of Ni based mesoporous alumina by Co incorporation in conversion of biogas to synthesis gas. *Appl. Catal. B* **2016**, *198*, 254–265. [CrossRef]
141. Nguyen, T.H.; Łamacz, A.; Krztoń, A.; Djéga-Mariadassou, G. Partial oxidation of methane over Ni_0/La_2O_3 bifunctional catalyst IV: Simulation of methane total oxidation, dry reforming and partial oxidation using the Quasi-Steady State Approximation. *Appl. Catal. B* **2016**, *199*, 424–432. [CrossRef]

142. García-Vargas, J.M.; Valverde, J.L.; Lucas-Consuegra, A.D.; Gomez-Monedero, B.; Dorado, F.; Sanchez, P. Methane tri-reforming over a Ni/β-SiC-based catalyst: Optimizing the feedstock composition. *Int. J. Hydrogen Energy* **2013**, *38*, 4524–4532. [CrossRef]
143. Tomishige, K.; Yamazaki, O.; Chen, Y.G.; Yokoyama, K.; Li, X.H.; Fujimoto, K. Development of ultra-stable Ni catalysts for CO_2 reforming of methane. *Catal. Today* **1998**, *45*, 35–39. [CrossRef]
144. Yu, M.; Zhu, K.; Liu, Z.; Xiao, H.; Deng, W.; Zhou, X. Carbon dioxide reforming of methane over promoted $Ni_xMg_{1-x}O$ (1 1 1) platelet catalyst derived from solvothermal synthesis. *Appl. Catal. B* **2014**, *148–149*, 177–190. [CrossRef]
145. Horváth, A.; Guczi, L.; Kocsonya, A.; Safran, G.; Parola, V.L.; Liotta, L.F.; Pantaleo, G.; Venezia, A.M. Sol-derived AuNi/$MgAl_2O_4$ catalysts: Formation, structure and activity in dry reforming of methane. *Appl. Catal. A* **2013**, *468*, 250–259. [CrossRef]
146. Wang, H.; Miller, J.T.; Shakouri, M.; Xi, C.; Wu, T.; Zhao, H.; Akatay, M.C. XANES and EXAFS studies on metal nanoparticle growth and bimetallic interaction of Ni-based catalysts for CO_2 reforming of CH_4. *Catal. Today* **2013**, *207*, 3–12. [CrossRef]
147. Li, Z.W.; Kawi, S. Multi-Ni@Ni phyllosilicate hollow sphere for CO_2 reforming of CH_4: Influence of Ni precursors on structure, sintering, and carbon resistance. *Catal. Sci. Technol.* **2018**, *8*, 1915–1922. [CrossRef]
148. Li, Z.W.; Jiang, B.; Wang, Z.G.; Kawi, S. High carbon resistant Ni@Ni phyllosilicate@SiO_2 core shell hollow sphere catalysts for low temperature CH_4 dry reforming. *J. CO_2 Util.* **2018**, *27*, 238–246. [CrossRef]
149. Li, Z.; Kathiraser, Y.; Kawi, S. Facile Synthesis of High Surface Area Yolk–Shell Ni@Ni Embedded SiO_2 via Ni Phyllosilicate with Enhanced Performance for CO_2 Reforming of CH_4. *ChemCatChem* **2015**, *7*, 160–168. [CrossRef]
150. Gao, X.Y.; Hidajat, K.; Kawi, S. Facile synthesis of Ni/SiO_2 catalyst by sequential hydrogen/air treatment: A superior anti-coking catalyst for dry reforming of methane. *J. CO_2 Util.* **2016**, *15*, 146–153. [CrossRef]
151. Choi, H.; Oh, S.; Tran, S.B.T.; Park, J.Y. Size-controlled model Ni catalysts on Ga_2O_3 for CO_2 hydrogenation to methanol. *J. Catal.* **2019**, *376*, 68–76. [CrossRef]
152. Li, Y.M.; Wang, Z.J.; Zhang, B.; Liu, Z.G.; Yang, T.X. Dry Reforming of Methane (DRM) by Highly Active and Stable Ni Nanoparticles on Renewable Porous Carbons. *Catalysts* **2020**, *10*, 501. [CrossRef]
153. Zhang, Q.; Zhang, T.; Shi, Y.; Zhao, B.; Wang, M.; Liu, Q.; Wang, J.; Long, K.; Duan, Y.; Ning, P. A sintering and carbon-resistant Ni-SBA-15 catalyst prepared by solid-state grinding method for dry reforming of methane. *J. CO_2 Util.* **2017**, *17*, 10–19. [CrossRef]
154. Zhang, Q.L.; Sun, M.H.; Ning, P.; Long, K.X.; Wang, J.; Tang, T.; Fan, J.; Sun, H.Y.; Yin, L.T.; Lin, Q. Effect of thermal induction temperature on re-dispersion behavior of Ni nanoparticles over Ni/SBA-15 for dry reforming of methane. *Appl. Surf. Sci.* **2019**, *469*, 368–377. [CrossRef]
155. Kang, D.; Lim, S.H.; Lee, J.W. Enhanced catalytic activity of methane dry reforming by the confinement of Ni nanoparticles into mesoporous silica. *Int. J. Hydrogen Energy* **2017**, *42*, 11270–11282. [CrossRef]
156. Baktash, E.; Littlewood, P.; Pfrommer, J.; Schomäcker, R.; Driess, M.; Thomas, A. Controlled Formation of Nickel Oxide Nanoparticles on Mesoporous Silica using Molecular Ni_4O_4 Clusters as Precursors: Enhanced Catalytic Performance for Dry Reforming of Methane. *ChemCatChem* **2015**, *7*, 1280–1284. [CrossRef]
157. Qian, L.; Huang, K.; Wang, H.; Kung, M.C.; Kung, H.H.; Li, J.; Chen, G.; Du, Q. Evaluation of the catalytic surface of Ni impregnated meso-microporous silica KIT-6 in CH_4 dry reforming by inverse gas chromatography. *Microporous Mesoporous Mater.* **2017**, *243*, 301–310. [CrossRef]
158. Wang, M.; Zhang, Q.; Zhang, T.; Wang, Y.; Wang, J.; Long, K.; Song, Z.; Liu, X.; Ning, P. Facile one-pot synthesis of highly dispersed Ni nanoparticles embedded in HMS for dry reforming of methane. *Chem. Eng. J.* **2017**, *313*, 1370–1381. [CrossRef]
159. Xin, J.; Cui, H.; Cheng, Z.; Zhou, Z. Bimetallic Ni-Co/SBA-15 catalysts prepared by urea co-precipitation for dry reforming of methane. *Appl. Catal. A* **2018**, *554*, 95–104. [CrossRef]
160. Guo, Y.H.; Xia, C.; Liu, B.S. Catalytic properties and stability of cubic mesoporous $La_xNi_yO_z$/KIT-6 catalysts for CO_2 reforming of CH_4. *Chem. Eng. J.* **2014**, *237*, 421–429. [CrossRef]
161. Liu, D.; Quek, X.Y.; Cheo, W.N.E.; Lau, R.; Borgna, A.; Yang, Y. MCM-41 supported nickel-based bimetallic catalysts with superior stability during carbon dioxide reforming of methane: Effect of strong metal–support interaction. *J. Catal.* **2009**, *266*, 380–390. [CrossRef]
162. Liu, D.; Quek, X.Y.; Adeline, H.H.; Zeng, G.; Li, Y.; Yang, Y. Carbon dioxide reforming of methane over nickel-grafted SBA-15 and MCM-41 catalysts. *Catal. Today* **2009**, *148*, 243–250. [CrossRef]

163. Baudouin, D.; Szeto, K.C.; Laurent, P.; Mallman, A.D.; Fenet, B.; Veyre, L.; Rodemerck, U.; Copéret, C.; Thieuleux, C. Nickel–Silicide Colloid Prepared under Mild Conditions as a Versatile Ni Precursor for More Efficient CO_2 Reforming of CH_4 Catalysts. *J. Am. Chem. Soc.* **2012**, *134*, 20624–20627. [CrossRef] [PubMed]
164. Xie, T.; Shi, L.; Zhang, J.; Zhang, D. Immobilizing Ni nanoparticles to mesoporous silica with size and location control via a polyol-assisted route for coking- and sintering-resistant dry reforming of methane. *Chem. Commun.* **2014**, *50*, 7250–7253. [CrossRef] [PubMed]
165. Gao, X.Y.; Liu, H.J.; Hidajat, K.; Kawi, S. Anti-Coking Ni/SiO_2 Catalyst for Dry Reforming of Methane: Role of Oleylamine/Oleic Acid Organic Pair. *ChemCatChem* **2015**, *7*, 4188–4196. [CrossRef]
166. Gao, X.Y.; Tan, Z.W.; Hidajat, K.; Kawi, S. Highly reactive Ni-Co/SiO_2 bimetallic catalyst via complexation with oleylamine/oleic acid organic pair for dry reforming of methane. *Catal. Today* **2017**, *281*, 250–258. [CrossRef]
167. Xu, L.; Song, H.; Chou, L. Carbon dioxide reforming of methane over ordered mesoporous NiO–MgO–Al_2O_3 composite oxides. *Appl. Catal. B* **2011**, *108–109*, 177–190. [CrossRef]
168. Xu, L.; Song, H.; Chou, L. Mesoporous nanocrystalline ceria–zirconia solid solutions supported nickel based catalysts for CO_2 reforming of CH_4. *Int. J. Hydrogen Energy* **2012**, *37*, 18001–18020. [CrossRef]
169. Xu, L.; Miao, Z.; Song, H.; Chen, W.; Chou, L. Significant roles of mesostructure and basic modifier for ordered mesoporous Ni/CaO–Al_2O_3 catalyst towards CO_2 reforming of CH_4. *Catal. Sci. Technol.* **2014**, *4*, 1759–1770. [CrossRef]
170. Ashcroft, A.T.; Cheetham, A.K.; Green, M.L.H.; Vernon, P.D.F. Partial oxidation of methane to synthesis gas using carbon dioxide. *Nature* **1991**, *352*, 225–226. [CrossRef]
171. Wang, N.; Xu, Z.; Deng, J.; Shen, K.; Yu, X.; Qian, W.; Chu, W.; Wei, F. One-pot Synthesis of Ordered Mesoporous NiCeAl Oxide Catalysts and a Study of Their Performance in Methane Dry Reforming. *ChemCatChem* **2014**, *6*, 1470–1480. [CrossRef]
172. Fakeeha, A.H.; Khan, W.U.; Al-Fatesh, A.S.; Abasaeed, A.E. Stabilities of zeolite-supported Ni catalysts for dry reforming of methane. *Chin. J. Catal.* **2013**, *34*, 764–768. [CrossRef]
173. Dai, C.; Zhang, S.; Zhang, A.; Song, C.; Shi, C.; Guo, X. Hollow zeolite encapsulated Ni–Pt bimetals for sintering and coking resistant dry reforming of methane. *J. Mater. Chem. A* **2015**, *3*, 16461–16468. [CrossRef]
174. Yin, Y.; Rioux, R.M.; Erdonmez, C.K.; Hughes, S.; Somorjai, G.A.; Alivisatos, A.P. Formation of Hollow Nanocrystals Through the Nanoscale Kirkendall Effect. *Science* **2004**, *304*, 711–714. [CrossRef] [PubMed]
175. Park, J.C.; Bang, J.U.; Lee, J.; Ko, C.H.; Song, H. Ni@SiO_2yolk-shell nanoreactor catalysts: High temperature stability and recyclability. *J. Mater. Chem.* **2010**, *20*, 1239–1246. [CrossRef]
176. Kim, D.H.; Kim, S.Y.; Han, S.W.; Cho, Y.K.; Jeong, M.-G.; Park, E.J.; Kim, Y.D. The catalytic stability of TiO_2-shell/Ni-core catalysts for CO_2 reforming of CH_4. *Appl. Catal. A* **2015**, *495*, 184–191.
177. Lu, Y.; Guo, D.; Ruan, Y.Z.; Zhao, Y.J.; Wang, S.P.; Ma, X.B. Facile one-pot synthesis of Ni@HSS as a novel yolk-shell structure catalyst for dry reforming of methane. *J. CO_2 Util.* **2018**, *24*, 190–199. [CrossRef]
178. Li, Z.W.; Kawi, S. Facile Synthesis of Multi-Ni-Core@Ni Phyllosilicate@CeO_2 Shell Hollow Spheres with High Oxygen Vacancy Concentration for Dry Reforming of CH_4. *ChemCatChem* **2018**, *10*, 2994–3001. [CrossRef]
179. Cao, Y.; Lu, M.R.; Fang, J.H.; Shi, L.Y.; Zhang, D.S. Hexagonal boron nitride supported mesoSiO_2-confined Ni catalysts for dry reforming of methane. *Chem. Commun.* **2017**, *53*, 7549–7552. [CrossRef]
180. Tian, J.Q.; Ma, B.; Bu, S.Y.; Yuan, Q.H.; Zhao, C. One-pot synthesis of highly sintering- and coking-resistant Ni nanoparticles encapsulated in dendritic mesoporous SiO_2 for methane dry reforming. *Chem. Commun.* **2018**, *54*, 13993–13996. [CrossRef]
181. Dou, J.; Zhang, R.G.; Hao, X.B.; Bao, Z.H.; Wu, T.P.; Wang, B.J.; Yu, F. Sandwiched SiO_2@Ni@ZrO_2 as a coke resistant nanocatalyst for dry reforming of methane. *Appl. Catal. B* **2019**, *254*, 612–623. [CrossRef]
182. Bian, Z.F.; Kawi, S. Sandwich-Like Silica@Ni@Silica Multicore–Shell Catalyst for the Low-Temperature Dry Reforming of Methane: Confinement Effect Against Carbon Formation. *ChemCatChem* **2018**, *10*, 320–328. [CrossRef]
183. Zhang, J.; Li, F. Coke-resistant Ni@SiO_2 catalyst for dry reforming of methane. *Appl. Catal. B* **2015**, *176–177*, 513–521. [CrossRef]
184. Li, Z.; Mo, L.; Kathiraser, Y.; Kawi, S. Yolk–Satellite–Shell Structured Ni–Yolk@Ni@SiO_2 Nanocomposite: Superb Catalyst toward Methane CO_2 Reforming Reaction. *ACS Catal.* **2014**, *4*, 1526–1536. [CrossRef]

185. Peng, X.Z.H.; Zhang, L.; Rao, C.; Lian, J.; Liu, W.; Ying, G.Z.J.; Wang, Z.; Zhang, N.; Wang, X. One-Pot Facile Fabrication of Multiple Nickel Nanoparticles Confined in Microporous Silica Giving a Multiple-Cores@Shell Structure as a Highly Efficient Catalyst for Methane Dry Reforming. *ChemCatChem* **2017**, *9*, 127–136. [CrossRef]
186. Han, J.W.; Kim, C.; Park, J.S.; Lee, H. Highly Coke-Resistant Ni Nanoparticle Catalysts with Minimal Sintering in Dry Reforming of Methane. *ChemSusChem* **2014**, *7*, 451–456. [CrossRef]
187. Li, Z.W.; Kathiraser, Y.; Ashok, J.; Oemar, U.; Kawi, S. Simultaneous Tuning Porosity and Basicity of Nickel@Nickel–Magnesium Phyllosilicate Core–Shell Catalysts for CO_2 Reforming of CH_4. *Langmuir* **2014**, *30*, 14694–14705. [CrossRef]
188. Bian, Z.F.; Suryawinata, I.Y.; Kawi, S. Highly carbon resistant multicore-shell catalyst derived from Ni-Mg phyllosilicate nanotubes@silica for dry reforming of methane. *Appl. Catal. B* **2016**, *195*, 1–8. [CrossRef]
189. Du, X.; Zhang, D.; Gao, R.; Huang, L.; Shi, L.; Zhang, J. Design of modular catalysts derived from NiMgAl-LDH@m-SiO_2 with dual confinement effects for dry reforming of methane. *Chem. Commun.* **2013**, *49*, 6770–6772. [CrossRef]
190. Wu, T.; Cai, W.; Zhang, P.; Song, X.; Gao, L. Cu–Ni@SiO_2 alloy nanocomposites for methane dry reforming catalysis. *RSC Adv.* **2013**, *3*, 23976–23979. [CrossRef]
191. Zhao, Y.; Li, H.; Li, H. NiCo@SiO_2 core-shell catalyst with high activity and long lifetime for CO_2 conversion through DRM reaction. *Nano Energy* **2018**, *45*, 101–108. [CrossRef]
192. Chen, T.; Wang, Z.; Hu, J.; Wai, M.H.; Kawi, S.; Lin, Y.S. High CO_2 permeability of ceramic-carbonate dual-phase hollow fiber membrane at medium-high temperature. *J. Membr. Sci.* **2020**, *597*, 117770. [CrossRef]
193. Yang, T.N.; Kathiraser, Y.; Kawi, S. $La_{0.6}Sr_{0.4}Co_{0.8}Ni_{0.2}O_{3-\delta}$ hollow fiber membrane reactor: Integrated oxygen separation—CO_2 reforming of methane reaction for hydrogen production. *Int. J. Hydrogen Energy* **2013**, *38*, 4483–4491. [CrossRef]
194. Chen, T.; Wang, Z.; Das, S.; Liu, L.; Li, Y.; Kawi, S.; Lin, Y.S. A novel study of sulfur-resistance for CO_2 separation through asymmetric ceramic-carbonate dual-phase membrane at high temperature. *J. Membr. Sci.* **2019**, *581*, 72–81. [CrossRef]